Inverse elastic surface scattering with near-field data*

Peijun Li, Yuliang Wang and Yue Zhao

Department of Mathematics, Purdue University, West Lafayette, IN 47907, USA

E-mail: lipeijun@purdue.edu, wang2049@purdue.edu and zhao399@purdue.edu

CrossMark

Abstract

Consider the scattering of a time-harmonic plane wave by a one-dimensional periodic surface. A novel computational method is proposed for solving the inverse elastic surface scattering problem by using the near-field data. Above the surface, the space is filled with a homogeneous and isotropic elastic medium, while the space below the surface is assumed to be elastically rigid. Given an incident field, the inverse problem is to reconstruct the surface from the displacement of the wave field at a horizontal line above the surface. This paper is a nontrivial extension of the authors' recent work on near-field imaging of the Helmholtz equation and the Maxwell equation to the more complicated Navier equation due to coexistence of the compressional and shear waves that propagate at different speed. Based on the Helmholtz decomposition, the wave field is decomposed into its compressional and shear parts by using two scalar potential functions. The transformed field expansion is then applied to each component and a coupled recurrence relation is obtained for their power series expansions. By solving the coupled system in the frequency domain, simple and explicit reconstruction formulas are derived for two types of measurement data. The method requires only a single illumination with a fixed frequency and incident angle. Numerical experiments show that it is simple, effective, and efficient to reconstruct the scattering surfaces with subwavelength resolution.

Keywords: inverse elastic surface scattering, near-field imaging, subwavelength resolution

(Some figures may appear in colour only in the online journal)

1. Introduction

The elastic wave scattering problems have received much attention from both the engineering and mathematical communities for their significant applications in diverse scientific areas such as geophysics, seismology, and nondestructive testing [1–4, 14, 22, 23, 25, 28, 29]. For instance, they are fundamental to detect the fractures in sedimentary rocks for the production of underground gas and liquids. Moreover, for the investigation of earthquake and the detection of oil and ore bodies, they have played an important role in the problem for elastic pulse transmission and reflection through the Earth. Given an incident field, the direct scattering problem is to predict the scattered field by a known scatterer, e.g. a rough surface, an obstacle, or an inhomogeneous medium. Conversely, the inverse scattering problem is to recover the properties of the scatterer such as its geometry or material, from the measurement data of the wave field. This paper is aimed at developing an effective mathematical model and design an efficient computational method for solving quantitatively an inverse elastic scattering problem of reconstructing the shape of rough surfaces.

Specifically, we consider the scattering of a time-harmonic plane wave incident on a one-dimensional periodic surface. The space above the surface is filled with a homogeneous and isotropic elastic medium; while the space below the surface is assumed to be elastically rigid. Given an incident elastic plane wave, the inverse problem is to determine the surface from the wave field measured on a horizontal line above the surface. Although we focus on the periodic surfaces in this work, the method works for other types of surfaces which include the infinite/unbounded rough surfaces and the locally perturbed plane surfaces. We assume that the surface has a small amplitude comparing with the wavelength of the incident field, which is a suitable assumption in the scenario of near-field imaging. Since the space is assumed to be elastically rigid below the surface, we consider the simplest homogeneous Dirichlet boundary condition on the surface. The method can be naturally extended to surfaces with other boundary conditions, or the transmission problem where the wave can penetrate the surface into the substrate, as well as the obstacle problem where the surface is bounded and closed. These problems will be reported in future work.

The direct scattering problem has been investigated extensively by many researchers for either infinite rough surfaces [8, 9, 19–21] or periodic surfaces [6, 7, 17, 18]. The inverse problem has also been studied theoretically for its uniqueness [5] and numerically by using an optimization method [18] and the factorization method [24]. The optimization method is a common approach for solving many inverse problems and is criticized for its large computational complexity. As a quantitative method, it is accurate but requires a good initial guess and suffers from the issue of local minima. As a qualitative method, the factorization method is computationally efficient and requires no *a priori* information about the solution but it is not as accurate as those quantitative based methods.

Recently, a novel approach has been developed for solving a wide range of inverse surface scattering problems in the applications of near-field imaging by acoustic or electromagnetic waves, including impenetrable infinite rough surfaces [11], penetrable infinite rough surfaces [12], two- and three-dimensional diffraction gratings [10, 13, 15], bounded obstacles [26], and interior cavities [27]. This work is a nontrivial extension of the method from the Helmholtz and Maxwell equations, which describe the acoustic and electromagnetic wave propagation, to the Navier equation, which models the elastic wave propagation. The latter is more complicated due to the coexistence of compressional waves and shear waves that propagate at different speeds. In view of this physical characteristics, we use two scalar potential functions and split the wave field into its compressional and shear parts through the Helmholtz decomposition. The transparent boundary condition for each part can be derived
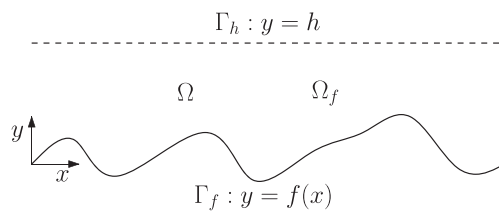
Figure 1. Problem geometry. The space below the scattering surface Γ_f is rigid and the space above Γ_f is filled with a homogeneous and isotropic elastic medium. An plane wave is incident on Γ_f from above and the total field is measured at the line Γ_h and used as the data for the inverse problem.

and the transparent boundary condition for the wave field can thus be deduced from the Helmholtz decomposition. We then apply the transformed field expansion on each part and obtain a coupled system of recursive boundary value problems formulated in a rectangular domain. The system is further reduced to the frequency domain through the Fourier series expansion and solved in an analytical form. Based on the analytic solutions, the nonlinear inverse problem is linearized by dropping higher order terms in the power series expansions; explicit reconstruction formulas are obtained in terms of the Fourier coefficients of the data and the solutions.

The method requires only a single incident field with one polarization, one frequency, and one incident direction. It is realized efficiently by using the fast Fourier transform (FFT). As a regularization technique to overcome the ill-posedness, the spectral cut-off is adopted to suppress the exponential growth of the noise in the evanescent wave components. Numerical results show that the method is simple, efficient, and effective to reconstruct rigid surfaces with subwavelength resolution. Numerical examples include both smooth and non-smooth surfaces, although the mathematical justification requires smooth surfaces. Numerical experiments investigate the effect of the reconstruction from all the parameters such as the deformation parameter, the measurement distance, and the noise level. To the best of our knowledge, this work provides the first quantitative method for solving the inverse elastic surface scattering problem with subwavelength resolution.

The outline of this paper is as follows. In section 2, we introduce the mathematical model for elastic surface scattering and derive the boundary value problems. Section 3 is devoted to the transformed field expansion and the analytical solution to the coupled system in the frequency domain. The reconstruction formulas are presented in section 4, where two different formulas are given depending on two different type of measurement data. In section 5, we report numerical examples to demonstrate the effectiveness of the proposed method. Some general remarks and directions for future research are concluded in section 6.

2. A model problem

In this section, we introduce a mathematical model, define some notation, and deduce a reduced boundary value problem for the elastic scattering by a rough surface. For simplicity of presentation, we take a periodic surface for an example, which is also known as a diffraction grating problem. The results can be obtained similarly for an infinite/unbounded surface and a locally perturbed planar surface by considering the Fourier transform instead of the Fourier series expansion.

2.1. Elastic wave equation

Let us first introduce the problem geometry. As seen in figure 1, we consider a periodic surface within one period of Λ. The surface is assumed to be invariant in the z-direction. Let the cross section of the surface be described by $\Gamma_f = \{(x, y) \in \mathbb{R}^2 \colon y = f(x), \ 0 < x < \Lambda\}$, where $f \in C^2(\mathbb{R})$ is a periodic function with period Λ and has the form

$$f(x) = \varepsilon g(x). \tag{2.1}$$

Here $\varepsilon > 0$, standing for the surface deformation parameter, is a sufficiently small constant. The periodic function $g \in C^2(\mathbb{R})$ describes the surface profile and has the same period of Λ.

Denote by $\Omega_f = \{(x, y) \in \mathbb{R}^2 \colon y > f(x), \ 0 < x < \Lambda\}$ the space above Γ_f, which is filled with a homogeneous and isotropic elastic medium. Denote $\Omega = \{(x, y) \in \mathbb{R}^2 \colon f(x) < y < h\}$ and $\Gamma_h = \{(x, y) \in \mathbb{R}^2 \colon y = h, \ 0 < x < \Lambda\}$, where $h > \max_{x \in (0, \Lambda)} f(x)$ is the measurement distance constant.

Let $\boldsymbol{u}^{\text{inc}}$ be a time-harmonic plane wave which is incident on the scattering surface Γ_f from above in Ω_f. More explicitly, the incident wave can be either the compressional wave

$$\boldsymbol{u}_{\text{p}}^{\text{inc}} = [\sin\theta, \ -\cos\theta]\mathrm{e}^{\mathrm{i}\kappa_{\text{p}}(x\sin\theta - y\cos\theta)}$$

or the shear wave

$$\boldsymbol{u}_{\text{s}}^{\text{inc}} = [\cos\theta, \ \sin\theta]\mathrm{e}^{\mathrm{i}\kappa_{\text{s}}(x\sin\theta - y\cos\theta)},$$

where $\theta \in (-\pi/2, \ \pi/2)$ is the incident angle, and

$$\kappa_{\text{p}} = \omega \big/ \sqrt{\lambda + 2\mu}, \quad \kappa_{\text{s}} = \omega \big/ \sqrt{u} \tag{2.2}$$

are the compressional and shear wavenumbers, respectively. Here $\omega > 0$ is the angular frequency, λ and μ are the Lamé constants satisfying $\mu > 0$ and $\lambda + \mu > 0$ which implies that $\kappa_{\text{p}} < \kappa_{\text{s}}$. For the sake of determinacy and simplicity in the presentation of this paper, we take the incident wave to be the compressional plane wave with normal incidence, i.e.,

$$\boldsymbol{u}^{\text{inc}} = [0, \ -1]\mathrm{e}^{-\mathrm{i}\kappa_{\text{p}}y}. \tag{2.3}$$

The method works for general non-normal incidence and the shear plane wave with obvious modifications. It can be verified that the incident field $\boldsymbol{u}^{\text{inc}}$ satisfies the two-dimensional Navier equation:

$$\mu\Delta\boldsymbol{u}^{\text{inc}} + (\lambda + \mu)\nabla\nabla \cdot \boldsymbol{u}^{\text{inc}} + \omega^2\boldsymbol{u}^{\text{inc}} = 0 \quad \text{in } \Omega_f. \tag{2.4}$$

Since the structure is invariant in the z-direction, the displacement of the total field $\boldsymbol{u}$ satisfies the same Navier equation:

$$\mu\Delta\boldsymbol{u} + (\lambda + \mu)\nabla\nabla \cdot \boldsymbol{u} + \omega^2\boldsymbol{u} = 0 \quad \text{in } \Omega_f. \tag{2.5}$$

By assuming that the substrate below Γ_f is impenetrable and rigid, we have

$$\boldsymbol{u} = 0 \quad \text{on } \Gamma_f. \tag{2.6}$$

The total field $\boldsymbol{u}$ consists of the incident field $\boldsymbol{u}^{\text{inc}}$ and the scattered field $\boldsymbol{v}$:

$$\boldsymbol{u} = \boldsymbol{u}^{\text{inc}} + \boldsymbol{v},$$

where the scattered field $\boldsymbol{v}$ is required to satisfy the bounded outgoing wave condition as $y \to \infty$.

It is clear to note that the two components of the wavefield are coupled in the Navier equation, which is the essential difficulty to derive an analytic solution when applying the

transformed field expansion. To decouple them, it is crucial to introduce the Helmholtz decomposition to split the wavefield into its compressional and shear parts.

Let $\boldsymbol{u} = [u_1,\ u_2]$ and u be a vector and a scalar function, respectively. Introduce a scalar curl operator and a vector curl operator:

$$\mathrm{curl}\ \boldsymbol{u} = \partial_x u_2 - \partial_y u_1, \quad \mathbf{curl}\ u = \left[\ \partial_y u, \ -\partial_x u\right].$$

For any solution $\boldsymbol{u}$ of the Navier equation (2.5), the Helmholtz decomposition reads

$$\boldsymbol{u} = \nabla\phi + \mathbf{curl}\ \psi, \tag{2.7}$$

where ϕ and ψ are called the compressional and shear scalar potential functions. Substituting (2.7) into (2.5) yields

$$\nabla\left[\ (\lambda + 2\mu)\Delta\phi + \omega^2\phi\right] + \mathbf{curl}\left[\ \mu\Delta\psi + \omega^2\psi\right] = 0.$$

This equation is fulfilled if ϕ and ψ satisfy the homogeneous Helmholtz equations

$$\Delta\phi + \kappa_{\mathrm p}^2\phi = 0, \quad \Delta\psi + \kappa_{\mathrm s}^2\psi = 0, \tag{2.8}$$

where $\kappa_{\mathrm p}$ and $\kappa_{\mathrm s}$ are the compressional and shear wavenumbers defined in (2.2). Combining (2.7) and (2.8), we have the explicit representations of ϕ and ψ in terms of $\boldsymbol{u}$:

$$\phi = -\frac{1}{\kappa_{\mathrm p}^2}\nabla\cdot\boldsymbol{u}, \quad \psi = \frac{1}{\kappa_{\mathrm s}^2}\mathrm{curl}\ \boldsymbol{u}. \tag{2.9}$$

In addition, it follows from the Helmholtz decomposition (2.7) that the boundary condition (2.6) is equivalent to

$$\partial_x\phi + \partial_y\psi = 0, \quad \partial_y\phi - \partial_x\psi = 0 \quad \text{on}\ \Gamma_f. \tag{2.10}$$

Hence, we may either solve the boundary value problem of the Navier equation for $\boldsymbol{u}$ and then obtain the scalar potentials ϕ, ψ via (2.9), or solve the boundary value problem of the Helmholtz equations for ϕ, ψ and then obtain $\boldsymbol{u}$ by (2.7).

2.2. Transparent boundary conditions

To reduce the problem from the unbounded domain Ω_f into the bounded domain Ω, it is required to introduce transparent boundary conditions for $\boldsymbol{u}$ and for ϕ, ψ on Γ_h.

Subtracting (2.4) from (2.5), we get the Navier equation for the scattered field:

$$\mu\Delta\boldsymbol{v} + (\lambda + \mu)\nabla\nabla\cdot\boldsymbol{v} + \omega^2\boldsymbol{v} = 0 \quad \text{in}\ \Omega_f. \tag{2.11}$$

Similarly, we decompose the scattered field $\boldsymbol{v}$ into its compressional part and the shear part:

$$\boldsymbol{v} = \nabla\varphi + \mathbf{curl}\ \psi, \tag{2.12}$$

where the scalar potential functions

$$\varphi = -\frac{1}{\kappa_{\mathrm p}^2}\nabla\cdot\boldsymbol{v}, \quad \psi = \frac{1}{\kappa_{\mathrm s}^2}\mathrm{curl}\ \boldsymbol{v},$$

satisfy the homogeneous Helmholtz equations

$$\Delta\varphi + \kappa_{\mathrm p}^2\varphi = 0, \quad \Delta\psi + \kappa_{\mathrm s}^2\psi = 0. \tag{2.13}$$

Remark 2.1. Recalling that $\boldsymbol{u} = \boldsymbol{u}^{\mathrm{inc}} + \boldsymbol{v}$, we may also decompose the scalar potentials ϕ, ψ into their incident and scattered fields:

$$\phi = \phi^{\text{inc}} + \varphi, \quad \psi = \psi^{\text{inc}} + \psi.$$

Below, we shall show that $\psi^{\text{inc}} = 0$ so the total field ψ is equal to the scattered field ψ.

It follows from the uniqueness of the solution for the direct problem that φ, ψ are periodic functions and admit the Fourier series expansions

$$\varphi(x, y) = \sum_{n \in \mathbb{Z}} \varphi^{(n)}(y) e^{i\alpha_n x}, \quad \psi(x, y) = \sum_{n \in \mathbb{Z}} \psi^{(n)}(y) e^{i\alpha_n x}, \tag{2.14}$$

where $\alpha_n = 2n\pi/\Lambda$. Plugging (2.14) into (2.13) yields

$$\frac{d^2 \varphi^{(n)}(y)}{dy^2} + \left(\beta_{\text{p}}^{(n)}\right)^2 \varphi^{(n)}(y) = 0, \quad \frac{d^2 \psi^{(n)}(y)}{dy^2} + \left(\beta_{\text{s}}^{(n)}\right)^2 \psi^{(n)}(y) = 0, \tag{2.15}$$

where

$$\beta_{\text{p}}^{(n)} = \begin{cases} \left(\kappa_{\text{p}}^2 - \alpha_n^2\right)^{1/2}, & |\alpha_n| < \kappa_{\text{p}}, \\ i\left(\alpha_n^2 - \kappa_{\text{p}}^2\right)^{1/2}, & |\alpha_n| > \kappa_{\text{p}}, \end{cases} \quad \beta_{\text{s}}^{(n)} = \begin{cases} \left(\kappa_{\text{s}}^2 - \alpha_n^2\right)^{1/2}, & |\alpha_n| < \kappa_{\text{s}}, \\ i\left(\alpha_n^2 - \kappa_{\text{s}}^2\right)^{1/2}, & |\alpha_n| > \kappa_{\text{s}}. \end{cases} \tag{2.16}$$

Following from the bounded outgoing radiation condition, we may obtain the analytic solutions of second order differential equation (2.15):

$$\varphi(x, y) = \sum_{n \in \mathbb{Z}} \varphi^{(n)}(h) e^{i\left(\alpha_n x + \beta_{\text{p}}^{(n)}(y-h)\right)}, \quad \psi(x, y) = \sum_{n \in \mathbb{Z}} \psi^{(n)}(h) e^{i\left(\alpha_n x + \beta_{\text{s}}^{(n)}(y-h)\right)}, \tag{2.17}$$

which are called the Rayleigh expansions of the scalar potential functions φ and ψ. Taking the partial derivatives with respect to y of (2.17) and evaluating at $y = h$, we get

$$\partial_y \varphi(x, h) = \sum_{n \in \mathbb{Z}} i\beta_{\text{p}}^{(n)} \varphi^{(n)}(h) e^{i\alpha_n x}, \quad \partial_y \psi(x, h) = \sum_{n \in \mathbb{Z}} i\beta_{\text{s}}^{(n)} \psi^{(n)}(h) e^{i\alpha_n x}. \tag{2.18}$$

For a given periodic function $v(x)$ with period Λ, it has the Fourier series expansion

$$v(x) = \sum_{n \in \mathbb{Z}} v^{(n)} e^{i\alpha_n x}, \quad v^{(n)} = \frac{1}{\Lambda} \int_0^\Lambda v(x) e^{-i\alpha_n x} dx.$$

We define two boundary operators

$$\left(\mathcal{B}_{\text{p}} v\right)(x) = \sum_{n \in \mathbb{Z}} i\beta_{\text{p}}^{(n)} v^{(n)} e^{i\alpha_n x}, \quad \left(\mathcal{B}_{\text{s}} v\right)(x) = \sum_{n \in \mathbb{Z}} i\beta_{\text{s}}^{(n)} v^{(n)} e^{i\alpha_n x}.$$

It is easy to verify from (2.18) that

$$\partial_y \varphi = \mathcal{B}_{\text{p}} \varphi, \quad \partial_y \psi = \mathcal{B}_{\text{s}} \psi \quad \text{on } \Gamma_h. \tag{2.19}$$

Recall (2.3) and the Helmholtz decomposition for the incident field

$$\boldsymbol{u}^{\text{inc}} = \nabla \phi^{\text{inc}} + \mathbf{curl}\, \psi^{\text{inc}},$$

which gives

$$\phi^{\text{inc}} = -\frac{1}{\kappa_{\text{p}}^2} \nabla \cdot \boldsymbol{u}^{\text{inc}} = -\frac{i}{\kappa_{\text{p}}} e^{-i\kappa_{\text{p}} y}, \quad \psi^{\text{inc}} = \frac{1}{\kappa_{\text{s}}^2} \operatorname{curl} \boldsymbol{u}^{\text{inc}} = 0.$$

A simple calculation yields

$$\partial_y \phi^{\text{inc}} = -e^{-i\kappa_{\text{p}} h}, \quad \mathcal{B}_{\text{p}} \phi^{\text{inc}} = e^{-i\kappa_{\text{p}} h} \quad \text{on } \Gamma_h. \tag{2.20}$$

Combining (2.19) and (2.20), we obtain the transparent boundary conditions for the scalar potential functions ϕ and ψ:

$$\partial_y \phi = \mathscr{B}_{\mathrm{p}} \phi + \rho, \quad \partial_y \psi = \mathscr{B}_{\mathrm{s}} \psi \quad \text{on } \Gamma_h, \tag{2.21}$$

where $\rho = -2\mathrm{e}^{-\mathrm{i}\kappa_{\mathrm{p}}h}$.

Next we derive the transparent boundary condition for the displacement of the total field $\boldsymbol{u}$. Given a vector field $\boldsymbol{v} = [v_1, \ v_2]$, we define a boundary operator on Γ_h:

$$\mathscr{T}\boldsymbol{v} = \mu\partial_y\boldsymbol{v} + (\lambda + \mu)[0, \ 1]\nabla\cdot\boldsymbol{v} = \Big[\mu\partial_y v_1, \ (\lambda+\mu)\partial_x v_1 + (\lambda+2\mu)\partial_y v_2\Big]. \tag{2.22}$$

Following from the Helmholtz decomposition (2.12) and the Rayleigh expansions for the scalar potential functions (2.17), we obtain the Rayleigh expansion for the scattered field $\boldsymbol{v}$:

$$\boldsymbol{v} = \sum_{n\in\mathbb{Z}}\mathrm{i}\Big[\alpha_n, \ \beta_{\mathrm{p}}^{(n)}\Big]\varphi^{(n)}(h)\mathrm{e}^{\mathrm{i}\left(\alpha_n x + \beta_{\mathrm{p}}^{(n)}(y-h)\right)} + \mathrm{i}\Big[\beta_{\mathrm{s}}^{(n)}, \ -\alpha_n\Big]\psi^{(n)}(h)\mathrm{e}^{\mathrm{i}\left(\alpha_n x + \beta_{\mathrm{s}}^{(n)}(y-h)\right)}. \tag{2.23}$$

On the other hand, as a periodic function, $\boldsymbol{v} = [v_1, \ v_2]$ admits the Fourier expansion

$$v_j(x, h) = \sum_{n\in\mathbb{Z}} v_j^{(n)}(h)\mathrm{e}^{\mathrm{i}\alpha_n x}. \tag{2.24}$$

Plugging (2.24) and (2.17) into (2.12), we obtain a system of algebraic equations for $\varphi^{(n)}$ and $\psi^{(n)}$:

$$\mathrm{i}\alpha_n\varphi^{(n)}(h) + \mathrm{i}\beta_{\mathrm{s}}^{(n)}\psi^{(n)}(h) = v_1^{(n)}(h),$$
$$\mathrm{i}\beta_{\mathrm{p}}^{(n)}\varphi^{(n)}(h) - \mathrm{i}\alpha_n\psi^{(n)}(h) = v_2^{(n)}(h).$$

An application of Cramer's rule yields

$$\varphi^{(n)}(h) = -\frac{\mathrm{i}\left(\alpha_n v_1^{(n)}(h) + \beta_{\mathrm{s}}^{(n)}v_2^{(n)}(h)\right)}{\alpha_n^2 + \beta_{\mathrm{p}}^{(n)}\beta_{\mathrm{s}}^{(n)}}, \quad \psi^{(n)}(h) = \frac{\mathrm{i}\left(\alpha_n v_2^{(n)}(h) - \beta_{\mathrm{p}}^{(n)}v_1^{(n)}(h)\right)}{\alpha_n^2 + \beta_{\mathrm{p}}^{(n)}\beta_{\mathrm{s}}^{(n)}}. \tag{2.25}$$

Remark 2.2. It is easy to note from (2.16) that $\alpha_n^2 + \beta_{\mathrm{p}}^{(n)}\beta_{\mathrm{s}}^{(n)} \neq 0$ for $|\alpha_n| < \kappa_{\mathrm{s}}$. When $|\alpha_n| > \kappa_{\mathrm{s}}$, we have

$$\alpha_n^2 + \beta_{\mathrm{p}}^{(n)}\beta_{\mathrm{s}}^{(n)} = \alpha_n^2 - \left(\alpha_n^2 - \kappa_{\mathrm{p}}^2\right)^{1/2}\left(\alpha_n^2 - \kappa_{\mathrm{s}}^2\right)^{1/2}$$
$$= \frac{\alpha_n^2\left(\kappa_{\mathrm{p}}^2 + \kappa_{\mathrm{s}}^2\right) - \kappa_{\mathrm{p}}^2\kappa_{\mathrm{s}}^2}{\alpha_n^2 + \left(\alpha_n^2 - \kappa_{\mathrm{p}}^2\right)^{1/2}\left(\alpha_n^2 - \kappa_{\mathrm{s}}^2\right)^{1/2}} > \frac{\kappa_{\mathrm{s}}^4}{2\alpha_n^2},$$

which shows that $\alpha_n^2 + \beta_{\mathrm{p}}^{(n)}\beta_{\mathrm{s}}^{(n)} \neq 0$ for $n \in \mathbb{Z}$.

Combining (2.22), (2.24), and (2.25), we deduce an explicit representation for the boundary operator $\mathscr{T}$: for a periodic function with Fourier expansion $\boldsymbol{v} = \sum_{n\in\mathbb{Z}}\boldsymbol{v}^{(n)}\mathrm{e}^{\mathrm{i}\alpha_n x}$, it holds

$$\mathscr{T}\boldsymbol{v} = \sum_{n\in\mathbb{Z}} \mathrm{i} \begin{bmatrix} \dfrac{\omega^2\beta_{\mathrm{p}}^{(n)}}{\alpha_n^2 + \beta_{\mathrm{p}}^{(n)}\beta_{\mathrm{s}}^{(n)}} & \mu\alpha_n - \dfrac{\omega^2\alpha_n}{\alpha_n^2 + \beta_{\mathrm{p}}^{(n)}\beta_{\mathrm{s}}^{(n)}} \\ \dfrac{\omega^2\alpha_n}{\alpha_n^2 + \beta_{\mathrm{p}}^{(n)}\beta_{\mathrm{s}}^{(n)}} - \mu\alpha_n & \dfrac{\omega^2\beta_{\mathrm{s}}^{(n)}}{\alpha_n^2 + \beta_{\mathrm{p}}^{(n)}\beta_{\mathrm{s}}^{(n)}} \end{bmatrix} \boldsymbol{v}^{(n)}\mathrm{e}^{\mathrm{i}\alpha_n x}. \quad (2.26)$$

A simple calculation yields

$$\mu\partial_y\boldsymbol{u}^{\mathrm{inc}} + (\lambda + \mu)[0,\ 1]\nabla\cdot\boldsymbol{u}^{\mathrm{inc}} = \mathrm{i}\kappa_{\mathrm{p}}(\lambda + 2\mu)[0,\ 1]\mathrm{e}^{-\mathrm{i}\kappa_{\mathrm{p}}h}$$

and

$$\mathscr{T}\boldsymbol{u}^{\mathrm{inc}} = -\mathrm{i}\kappa_{\mathrm{p}}(\lambda + 2\mu)[0,\ 1]\mathrm{e}^{-\mathrm{i}\kappa_{\mathrm{p}}h},$$

which yields the transparent boundary condition for the total field $\boldsymbol{u}$:

$$\mu\partial_y\boldsymbol{u} + (\lambda + \mu)[0,\ 1]\nabla\cdot\boldsymbol{u} = \mathscr{T}\boldsymbol{u} + \boldsymbol{\rho} \quad \text{on } \Gamma_h, \quad (2.27)$$

where

$$\boldsymbol{\rho} = 2\mathrm{i}\kappa_{\mathrm{p}}(\lambda + 2\mu)[0,\ 1]\mathrm{e}^{-\mathrm{i}\kappa_{\mathrm{p}}h}.$$

2.3. Reduced problem

Using the transparent boundary conditions, the elastic surface scattering can be reduced to a boundary value problem of the total field $\boldsymbol{u}$ in the bounded domain Ω:

$$\begin{cases} \mu\Delta\boldsymbol{u} + (\lambda + \mu)\nabla\nabla\cdot\boldsymbol{u} + \omega^2\boldsymbol{u} = 0, & \text{in } \Omega, \\ \boldsymbol{u} = 0, & \text{on } \Gamma_f, \\ \mu\partial_y\boldsymbol{u} + (\lambda + \mu)[0,\ 1]\nabla\cdot\boldsymbol{u} = \mathscr{T}\boldsymbol{u} + \boldsymbol{\rho}, & \text{on } \Gamma_h, \end{cases} \quad (2.28)$$

Due to the Helmholtz decomposition, we may alternatively consider the boundary value problem for the scalar potential functions ϕ and ψ in the bounded domain Ω:

$$\begin{cases} \Delta\phi + \kappa_{\mathrm{p}}^2\phi = 0, & \Delta\psi + \kappa_{\mathrm{s}}^2\psi = 0, & \text{in } \Omega, \\ \partial_x\phi + \partial_y\psi = 0, & \partial_y\phi - \partial_x\psi = 0, & \text{on } \Gamma_f, \\ \partial_y\phi = \mathscr{B}_{\mathrm{p}}\phi + \rho, & \partial_y\psi = \mathscr{B}_{\mathrm{s}}\psi, & \text{on } \Gamma_h. \end{cases} \quad (2.29)$$

Given the incident field, the direct problem is to solve the boundary value problem (2.28) or (2.29) for the known scattering surface function *f*. We refer to [17] for the mathematical study of the direct problem. The paper is focused on the inverse problem, which is to reconstruct *f* from the measurement of the total field on Γ_h, i.e., $\boldsymbol{u}(x, h)$. In particular, we are interested in the inverse problem in the near-field regime where the measurement distance *h* is much smaller than the wavelength $2\pi/\omega$.

We shall apply the transformed field expansion to (2.29) to derive an analytic solution for the direct problem and explicit reconstruction formulas for the inverse problem. To avoid the inverse crime, we shall solve directly (2.28) to obtain the synthetic data by using the finite element with perfectly matched layer (PML) technique.

3. Transformed field expansion

In this section, we introduce the transformed field expansion to derive an analytic solution for the coupled boundary value problem (2.29).

3.1. Change of variables

Consider the change of variables:

$$\tilde{x} = x, \quad \tilde{y} = h\left(\frac{y - f}{h - f}\right),$$

which maps the scattering surface Γ_f to the straight line $\Gamma_0 = \{(\tilde{x}, \tilde{y}) \in \mathbb{R}^2 : \tilde{y} = 0, \ 0 < \tilde{x} < \Lambda\}$, and maps the boundary Γ_h to itself. Hence the domain Ω is mapped into the rectangular domain $D = \{(\tilde{x}, \tilde{y}) \in \mathbb{R}^2 : 0 < \tilde{x} < \Lambda, \ 0 < \tilde{y} < h\}$.

The boundary value problem (2.29) will be reformulated in this transformed coordinates. It is easy to verify the differentiation rules

$$\partial_x = \partial_{\tilde{x}} - f'\left(\frac{h - \tilde{y}}{h - f}\right)\partial_{\tilde{y}},$$

$$\partial_y = \left(\frac{h}{h - f}\right)\partial_{\tilde{y}},$$

$$\partial_{xx} = \partial_{\tilde{x}\tilde{x}} + (f')^2\left(\frac{h - \tilde{y}}{h - f}\right)^2\partial_{\tilde{y}\tilde{y}} - 2f'\left(\frac{h - \tilde{y}}{h - f}\right)\partial_{\tilde{x}\tilde{y}}$$

$$\quad - \left[f''\left(\frac{h - \tilde{y}}{h - f}\right) + 2(f')^2\frac{(h - \tilde{y})}{(h - f)^2}\right]\partial_{\tilde{y}},$$

$$\partial_{yy} = \left(\frac{h}{h - f}\right)^2\partial_{\tilde{y}\tilde{y}}.$$

Introduce two new scalar potential functions $\tilde{\phi}(\tilde{x}, \tilde{y}) = \phi(x, y)$ and $\tilde{\psi}(\tilde{x}, \tilde{y}) = \psi(x, y)$ under the transformation. It can be verified that $\tilde{\phi}$ and $\tilde{\psi}$, upon dropping the tilde, satisfy the following partial differential equations in D:

$$\begin{cases} \left(c_1\partial_{xx} + c_2\partial_{yy} + c_3\partial_{xy} + c_4\partial_y + c_1\kappa_{\mathrm{p}}^2\right)\phi = 0, \\ \left(c_1\partial_{xx} + c_2\partial_{yy} + c_3\partial_{xy} + c_4\partial_y + c_1\kappa_{\mathrm{s}}^2\right)\psi = 0, \end{cases} \tag{3.1}$$

where

$$\begin{cases} c_1 = (h - f)^2, \\ c_2 = [f'(h - y)]^2 + h^2, \\ c_3 = -2f'(h - y)(h - f), \\ c_4 = -(h - y)\left[f''(h - f) + 2(f')^2\right]. \end{cases} \tag{3.2}$$

Under the change of variables, the boundary condition (2.10) becomes

$$
\begin{cases}
\left[\left(1 - h^{-1}f \right)\partial_x - f'\partial_y \right]\phi + \partial_y\psi = 0, \\
\partial_y\phi - \left[\left(1 - h^{-1}f \right)\partial_x - f'\partial_y \right]\psi = 0.
\end{cases}
\tag{3.3}
$$

The transparent boundary condition (2.21) reduces to

$$
\begin{cases}
\partial_y\phi = \left(1 - h^{-1}f \right)\left(\mathscr{B}_{\mathrm{p}}\phi + \rho \right), \\
\partial_y\psi = \left(1 - h^{-1}f \right)\mathscr{B}_{\mathrm{s}}\psi.
\end{cases}
\tag{3.4}
$$

3.2. Power series expansion

Noting the surface function (2.1), we consider formal expansions of ϕ and ψ in power series of the deformation parameter ε:

$$
\phi(x, y; \varepsilon) = \sum_{k=0}^{\infty}\phi_k(x, y)\varepsilon^k, \quad \psi(x, y; \varepsilon) = \sum_{k=0}^{\infty}\psi_k(x, y)\varepsilon^k.
\tag{3.5}
$$

Substituting (2.1) into (3.2) and plugging (3.5) into (3.1), we may obtain the recurrence equations for ϕ_k and ψ_k in D:

$$
\begin{cases}
\left(\Delta + \kappa_{\mathrm{p}}^2 \right)\phi_k = u_k, \\
\left(\Delta + \kappa_{\mathrm{s}}^2 \right)\psi_k = v_k,
\end{cases}
\tag{3.6}
$$

where

$$
\begin{cases}
u_k = \mathscr{D}_{\mathrm{p}}^{(1)}\phi_{k-1} + \mathscr{D}_{\mathrm{p}}^{(2)}\phi_{k-2}, \\
v_k = \mathscr{D}_{\mathrm{s}}^{(1)}\psi_{k-1} + \mathscr{D}_{\mathrm{s}}^{(2)}\psi_{k-2}.
\end{cases}
\tag{3.7}
$$

Here the differential operators

$$
\begin{aligned}
\mathscr{D}_{\mathrm{p}}^{(1)} &= h^{-1}\Big[2g\partial_{xx} + 2g'(h - y)\partial_{xy} + g''(h - y)\partial_y + 2\kappa_{\mathrm{p}}^2 g \Big], \\
\mathscr{D}_{\mathrm{p}}^{(2)} &= -h^{-2}\Big\{ g^2\partial_{xx} + (g')^2(h - y)^2\partial_{yy} + 2gg'(h - y)\partial_{xy} \\
&\quad - \Big[2(g')^2 - gg'' \Big](h - y)\partial_y + \kappa_{\mathrm{p}}^2 g^2 \Big\}, \\
\mathscr{D}_{\mathrm{s}}^{(1)} &= h^{-1}\Big[2g\partial_{xx} + 2g'(h - y)\partial_{xy} + g''(h - y)\partial_y + 2\kappa_{\mathrm{s}}^2 g \Big], \\
\mathscr{D}_{\mathrm{s}}^{(2)} &= -h^{-2}\Big\{ g^2\partial_{xx} + (g')^2(h - y)^2\partial_{yy} + 2gg'(h - y)\partial_{xy} \\
&\quad - \Big[2(g')^2 - gg'' \Big](h - y)\partial_y + \kappa_{\mathrm{s}}^2 g^2 \Big\}.
\end{aligned}
$$

Substituting (2.1) and (3.5) into (3.3), we obtain the recurrence equations for the boundary conditions on Γ_0:

$$
\begin{cases}
\partial_x\phi_k + \partial_y\psi_k = p_k, \\
\partial_y\phi_k - \partial_x\psi_k = q_k,
\end{cases}
\tag{3.8}
$$

where

$$\begin{cases} p_k = \left(h^{-1}g\partial_x + g'\partial_y\right)\phi_{k-1}, \\ q_k = -\left(h^{-1}g\partial_x + g'\partial_y\right)\psi_{k-1}. \end{cases} \tag{3.9}$$

Substituting (2.1) and (3.5) into (3.4), we derive the recurrence equations for the transparent boundary conditions on Γ_h:

$$\begin{cases} \left(\partial_y - \mathscr{B}_{\rm p}\right)\phi_k = r_k, \\ \left(\partial_y - \mathscr{B}_{\rm s}\right)\psi_k = s_k, \end{cases} \tag{3.10}$$

where

$$\begin{cases} r_0 = \rho, \quad r_1 = -h^{-1}g\left(\mathscr{B}_{\rm p}\phi_0 + \rho\right), \quad r_k = -h^{-1}g\mathscr{B}_{\rm p}\phi_{k-1}, \\ s_k = -h^{-1}g\mathscr{B}_{\rm s}\psi_{k-1}. \end{cases} \tag{3.11}$$

In all of the above recurrence equations, it is understood that ϕ_k, ψ_k, u_k, v_k, p_k, q_k, r_k, s_k are zeros when $k < 0$. The boundary value problem (3.6)–(3.11) for the current terms ϕ_k and ψ_k involve u_k, v_k, p_k, q_k, r_k, s_k, which depend only on previous two terms of ϕ_{k-1}, ϕ_{k-2} and ψ_{k-1}, ψ_{k-2}. Thus, the boundary value problem (3.6)–(3.11) can be recursively solved from $k = 0$.

3.3. Fourier series expansion

Since ϕ_k and ψ_k are periodic functions of x with period Λ, they have the Fourier series expansions

$$\phi_k(x, y) = \sum_{n\in\mathbb{Z}} \phi_k^{(n)}(y)\mathrm{e}^{\mathrm{i}\alpha_n x}, \quad \psi_k(x, y) = \sum_{n\in\mathbb{Z}} \psi_k^{(n)}(y)\mathrm{e}^{\mathrm{i}\alpha_n x}. \tag{3.12}$$

Substituting (3.12) into the boundary value problem (3.6)–(3.11), we obtain a coupled two-point boundary value problems:

$$\begin{cases} \partial_{yy}\phi_k^{(n)} + \left(\beta_{\rm p}^{(n)}\right)^2\phi_k^{(n)} = u_k^{(n)}, & 0 < y < h, \\ \partial_y\phi_k^{(n)} = q_k^{(n)} + \mathrm{i}\alpha_n\psi_k^{(n)}, & y = 0, \\ \partial_y\phi_k^{(n)} - \mathrm{i}\beta_{\rm p}^{(n)}\phi_k^{(n)} = r_k^{(n)}, & y = h, \end{cases} \tag{3.13}$$

and

$$\begin{cases} \partial_{yy}\psi_k^{(n)} + \left(\beta_{\rm s}^{(n)}\right)^2\psi_k^{(n)} = v_k^{(n)}, & 0 < y < h, \\ \partial_y\psi_k^{(n)} = p_k^{(n)} - \mathrm{i}\alpha_n\phi_k^{(n)}, & y = 0, \\ \partial_y\psi_k^{(n)} - \mathrm{i}\beta_{\rm s}^{(n)}\psi_k^{(n)} = s_k^{(n)}, & y = h, \end{cases} \tag{3.14}$$

where $u_k^{(n)}$, $v_k^{(n)}$, $p_k^{(n)}$, $q_k^{(n)}$, $r_k^{(n)}$, $s_k^{(n)}$ are the Fourier coefficients of u_k, v_k, p_k, q_k, r_k, s_k, respectively.

It follows from lemma appendix A.1 that the solutions of (3.13) and (3.14) are

$$\phi_k^{(n)}(y) = K_1\left(y; \beta_p^{(n)}\right)\left(q_k^{(n)} + i\alpha_n \psi_k^{(n)}(0)\right)$$
$$- K_2\left(y; \beta_p^{(n)}\right)r_k^{(n)} + \int_0^h K_3\left(y, z; \beta_p^{(n)}\right)u_k^{(n)}(z)\mathrm{d}z,$$

$$\psi_k^{(n)}(y) = K_1\left(y; \beta_s^{(n)}\right)\left(p_k^{(n)} - i\alpha_n \phi_k^{(n)}(0)\right)$$
$$- K_2\left(y; \beta_s^{(n)}\right)s_k^{(n)} + \int_0^h K_3\left(y, z; \beta_s^{(n)}\right)v_k^{(n)}(z)\mathrm{d}z,$$

where $\phi_k^{(n)}(0)$ and $\psi_k^{(n)}(0)$ are to be determined. Evaluating $\phi_k^{(n)}(y)$ and $\psi_k^{(n)}(y)$ at $y = 0$ in the above equations and recalling K_j in lemma appendix A.1, we obtain

$$\phi_k^{(n)}(0) = \frac{1}{i\beta_p^{(n)}}\left(q_k^{(n)} + i\alpha_n \psi_k^{(n)}(0)\right) - \frac{\mathrm{e}^{i\beta_p^{(n)}h}}{i\beta_p^{(n)}}r_k^{(n)} + \int_0^h \frac{\mathrm{e}^{i\beta_p^{(n)}z}}{i\beta_p^{(n)}}u_k^{(n)}(z)\mathrm{d}z,$$

$$\psi_k^{(n)}(0) = \frac{1}{i\beta_s^{(n)}}\left(p_k^{(n)} - i\alpha_n \phi_k^{(n)}(0)\right) - \frac{\mathrm{e}^{i\beta_s^{(n)}h}}{i\beta_s^{(n)}}s_k^{(n)} + \int_0^h \frac{\mathrm{e}^{i\beta_s^{(n)}z}}{i\beta_s^{(n)}}v_k^{(n)}(z)\mathrm{d}z,$$

which yields a system of algebraic equations for $\phi_k^{(n)}(0)$ and $\psi_k^{(n)}(0)$:

$$\begin{bmatrix} 1 & -\alpha_n\big/\beta_p^{(n)} \\ \alpha_n\big/\beta_s^{(n)} & 1 \end{bmatrix}\begin{bmatrix} \phi_k^{(n)}(0) \\ \psi_k^{(n)}(0) \end{bmatrix} = \begin{bmatrix} a_k^{(n)} \\ b_k^{(n)} \end{bmatrix}, \tag{3.15}$$

where

$$a_k^{(n)} = \left(i\beta_p^{(n)}\right)^{-1}\left(q_k^{(n)} - \mathrm{e}^{i\beta_p^{(n)}h}r_k^{(n)} + \int_0^h \mathrm{e}^{i\beta_p^{(n)}z}u_k^{(n)}(z)\mathrm{d}z\right),$$

$$b_k^{(n)} = \left(i\beta_s^{(n)}\right)^{-1}\left(p_k^{(n)} - \mathrm{e}^{i\beta_s^{(n)}h}s_k^{(n)} + \int_0^h \mathrm{e}^{i\beta_s^{(n)}z}v_k^{(n)}(z)\mathrm{d}z\right).$$

It follows from remark 2.2 that the linear system has a unique solution given by

$$\phi_k^{(n)}(0) = \left(\frac{\beta_p^{(n)}\beta_s^{(n)}}{\alpha_n^2 + \beta_p^{(n)}\beta_s^{(n)}}\right)\left(a_k^{(n)} + \frac{\alpha_n b_k^{(n)}}{\beta_p^{(n)}}\right),$$

$$\psi_k^{(n)}(0) = \left(\frac{\beta_p^{(n)}\beta_s^{(n)}}{\alpha_n^2 + \beta_p^{(n)}\beta_s^{(n)}}\right)\left(b_k^{(n)} - \frac{\alpha_n a_k^{(n)}}{\beta_s^{(n)}}\right).$$

Once $\phi_k^{(n)}(0)$ and $\psi_k^{(n)}(0)$ are determined, $\phi_k^{(n)}(y)$ and $\psi_k^{(n)}(y)$ are available for all k and n.

Next we shall deduce more explicit expressions for the leading terms $\phi_0^{(n)}(y)$, $\psi_0^{(n)}(y)$ and the linear terms $\phi_1^{(n)}(h)$, $\psi_1^{(n)}(h)$, which make it possible to derive the explicit reconstruction formulas.

3.4. Leading terms

For $k = 0$, it follows from (3.7), (3.9), and (3.11) that we obtain

$$u_0 = v_0 = p_0 = q_0 = s_0 = 0, \quad r_0 = \rho,$$

and their Fourier coefficients

$$u_0^{(n)} = v_0^{(n)} = p_0^{(n)} = q_0^{(n)} = s_0^{(n)} = 0, \quad r_0^{(n)} = \rho\delta_{0n}, \tag{3.16}$$

where δ is the Kronecker delta. Substituting (3.16) into (3.15) yields

$$a_0^{(n)} = -\rho\left(\frac{e^{i\beta_p^{(n)}h}}{i\beta_p^{(n)}}\right)\delta_{0n}, \quad b_0^{(n)} = 0.$$

and

$$\phi_0^{(n)}(0) = \rho\left(\frac{i\beta_s^{(n)}}{\alpha_n^2 + \beta_p^{(n)}\beta_s^{(n)}}\right)e^{i\beta_p^{(n)}h}\delta_{0n},$$

$$\psi_0^{(n)}(0) = -\rho\left(\frac{i\alpha_n}{\alpha_n^2 + \beta_p^{(n)}\beta_s^{(n)}}\right)e^{i\beta_p^{(n)}h}\delta_{0n},$$

which gives the Fourier coefficients of the leading terms

$$\phi_0^{(n)}(y) = \rho\left(\frac{e^{i\beta_p^{(n)}h}}{i\beta_p^{(n)}}\right)\left[\left(\frac{\alpha_n^2}{\alpha_n^2 + \beta_p^{(n)}\beta_s^{(n)}}\right)e^{i\beta_p^{(n)}y} - \frac{1}{2}\left(e^{i\beta_p^{(n)}y} + e^{-i\beta_p^{(n)}y}\right)\right]\delta_{0n},$$

$$\psi_0^{(n)}(y) = \rho\left(\frac{e^{i\beta_p^{(n)}h}}{i\beta_p^{(n)}}\right)\left(\frac{\alpha_n\beta_p^{(n)}}{\alpha_n^2 + \beta_p^{(n)}\beta_s^{(n)}}\right)e^{i\beta_s^{(n)}y}\delta_{0n}.$$

Plugging $\rho = -2e^{-i\kappa_p h}$ yields the explicit expressions of the leading terms:

$$\phi_0(x, y) = 2(i\kappa_p)^{-1}\cos(\kappa_p y), \quad \psi_0(x, y) = 0. \tag{3.17}$$

Remark 3.1. It follows from the Helmholtz decomposition (2.7) that

$$\boldsymbol{u} = \nabla\phi_0 + \mathbf{curl}\,\psi_0 = \left[\partial_x\phi_0, \ \partial_y\phi_0\right] + \left[\partial_y\psi_0, \ -\partial_x\psi_0\right]$$

$$= \left[0, \ 2i\sin(\kappa_p y)\right] = \left[0, \ e^{i\kappa_p y} - e^{-i\kappa_p y}\right].$$

If we denote by $\boldsymbol{u}^{\text{ref}} = [0, \ 1]e^{i\kappa_p y}$ the reflected field, then the total field is composed of the incident field $\boldsymbol{u}^{\text{inc}} = [0, \ -1]e^{-i\kappa_p y}$ and the reflected field, i.e., $\boldsymbol{u} = \boldsymbol{u}^{\text{inc}} + \boldsymbol{u}^{\text{ref}}$, which is consistent with the solution when a plane wave is incident on a flat surface.

3.5. Linear terms

For $k = 1$, it follows from (3.7), (3.9), (3.11), and (3.17) that we obtain

$$v_1 = p_1 = q_1 = s_1 = 0, \quad r_1 = -2ih^{-1}\sin(\kappa_p h)g(x),$$

$$u_1 = h^{-1}\left[-4i\kappa_p\cos(\kappa_p y)g(x) + 2i\sin(\kappa_p y)(h - y)g''(x)\right],$$

and their Fourier coefficients

$$v_1^{(n)} = p_1^{(n)} = q_1^{(n)} = s_1^{(n)} = 0, \quad r_1^{(n)} = -2ih^{-1} \sin\left(\kappa_{\mathrm{p}} h\right) g^{(n)},$$

$$u_1^{(n)} = h^{-1}\left[-4i\kappa_{\mathrm{p}} \cos\left(\kappa_{\mathrm{p}} y\right) - 2i\alpha_n^2 \sin\left(\kappa_{\mathrm{p}} y\right)(h - y)\right] g^{(n)},$$

where $g^{(n)}$ is the Fourier coefficient of the periodic function $g(x)$.

Substituting these Fourier coefficients to (3.15), we get

$$a_1^{(n)} = \left(i\beta_{\mathrm{p}}^{(n)}\right)^{-1}\left(-e^{i\beta_{\mathrm{p}}^{(n)}h} r_1^{(n)} + \int_0^h e^{i\beta_{\mathrm{p}}^{(n)}z} u_1^{(n)}(z)\,\mathrm{d}z\right), \quad b_1^{(n)} = 0,$$

and

$$\phi_1^{(n)}(0) = \frac{\beta_{\mathrm{s}}^{(n)}}{i\left(\alpha_n^2 + \beta_{\mathrm{p}}^{(n)}\beta_{\mathrm{s}}^{(n)}\right)}\left(-e^{i\beta_{\mathrm{p}}^{(n)}h} r_1^{(n)} + \int_0^h e^{i\beta_{\mathrm{p}}^{(n)}z} u_1^{(n)}(z)\,\mathrm{d}z\right),$$

$$\psi_1^{(n)}(0) = \frac{\alpha_n}{i\left(\alpha_n^2 + \beta_{\mathrm{p}}^{(n)}\beta_{\mathrm{s}}^{(n)}\right)}\left(e^{i\beta_{\mathrm{p}}^{(n)}h} r_1^{(n)} - \int_0^h e^{i\beta_{\mathrm{p}}^{(n)}z} u_1^{(n)}(z)\,\mathrm{d}z\right),$$

which gives the Fourier coefficients of the linear terms at $y = h$:

$$\phi_1^{(n)}(h) = \frac{\alpha_n^2 e^{i\beta_{\mathrm{p}}^{(n)}h}}{i\beta_{\mathrm{p}}^{(n)}\left(\alpha_n^2 + \beta_{\mathrm{p}}^{(n)}\beta_{\mathrm{s}}^{(n)}\right)}\left\{e^{i\beta_{\mathrm{p}}^{(n)}h} r_1^{(n)} + \frac{1}{2}\int_0^h\left[\alpha_n^{-2}\beta_{\mathrm{p}}^{(n)}\beta_{\mathrm{s}}^{(n)}\left(e^{i\beta_{\mathrm{p}}^{(n)}z} + e^{-i\beta_{\mathrm{p}}^{(n)}z}\right)\right.\right.$$

$$\left.\left. - \left(e^{i\beta_{\mathrm{p}}^{(n)}z} - e^{-i\beta_{\mathrm{p}}^{(n)}z}\right)\right]u_1^{(n)}(z)\,\mathrm{d}z\right\} - \frac{e^{i\beta_{\mathrm{p}}h}}{2i\beta_{\mathrm{p}}^{(n)}}\left(e^{i\beta_{\mathrm{p}}^{(n)}h} + e^{-i\beta_{\mathrm{p}}^{(n)}h}\right)r_1^{(n)},$$

$$\psi_1^{(n)}(h) = \frac{i\alpha_n e^{i\beta_{\mathrm{s}}^{(n)}h}}{\alpha_n^2 + \beta_{\mathrm{p}}^{(n)}\beta_{\mathrm{s}}^{(n)}}\left[-e^{i\beta_{\mathrm{p}}^{(n)}h} r_1^{(n)} + \int_0^h e^{i\beta_{\mathrm{p}}^{(n)}z} u_1^{(n)}(z)\,\mathrm{d}z\right].$$

We substitute the expression of $u_1^{(n)}$ into above integrals and obtain from the integration by parts that

$$\frac{1}{2}\int_0^h\left[\alpha_n^{-2}\beta_{\mathrm{p}}^{(n)}\beta_{\mathrm{s}}^{(n)}\left(e^{i\beta_{\mathrm{p}}^{(n)}z} + e^{-i\beta_{\mathrm{p}}^{(n)}z}\right) - \left(e^{i\beta_{\mathrm{p}}^{(n)}z} - e^{-i\beta_{\mathrm{p}}^{(n)}z}\right)\right]u_1^{(n)}(z)\,\mathrm{d}z = \left[ih^{-1}\sin\left(\kappa_{\mathrm{p}}h\right)\right.$$

$$\times\left(e^{i\beta_{\mathrm{p}}^{(n)}h} - e^{-i\beta_{\mathrm{p}}^{(n)}h}\right) - ih^{-1}\alpha_n^{-2}\beta_{\mathrm{p}}^{(n)}\beta_{\mathrm{s}}^{(n)}\sin\left(\kappa_{\mathrm{p}}h\right)$$

$$\times\left.\left(e^{i\beta_{\mathrm{p}}^{(n)}h} + e^{-i\beta_{\mathrm{p}}^{(n)}h}\right) - 2i\alpha_n^{-2}\kappa_{\mathrm{p}}\beta_{\mathrm{p}}^{(n)}\beta_{\mathrm{s}}^{(n)}\right]g^{(n)}$$

and

$$\int_0^h e^{i\beta_{\mathrm{p}}^{(n)}z} u_1^{(n)}(z)\,\mathrm{d}z = \left[-2i\kappa_{\mathrm{p}} - 2ih^{-1}e^{i\beta_{\mathrm{p}}^{(n)}h}\sin\left(\kappa_{\mathrm{p}}h\right)\right]g^{(n)}.$$

Finally, we substitute the expression of $r_1^{(n)}$ into above identities and deduce

$$
\begin{aligned}
\phi_1^{(n)}(h) ={}& \frac{\alpha_n^2 e^{i\beta_p^{(n)}h}}{i\beta_p^{(n)}\left(\alpha_n^2 + \beta_p^{(n)}\beta_s^{(n)}\right)} \left\{ e^{i\beta_p^{(n)}h}\left[-2ih^{-1}\sin\left(\kappa_p h\right)\right] \right. \\
&+ \left[ih^{-1}\sin\left(\kappa_p h\right)\left(e^{i\beta_p^{(n)}h} - e^{-i\beta_p^{(n)}h}\right) \right. \\
&\quad - ih^{-1}\alpha_n^{-2}\beta_p^{(n)}\beta_s^{(n)}\sin\left(\kappa_p h\right)\left(e^{i\beta_p^{(n)}h} + e^{-i\beta_p^{(n)}h}\right) \\
&\quad \left.\left. - 2i\alpha_n^{-2}\kappa_p\beta_p^{(n)}\beta_s^{(n)}\right]\right\} g^{(n)} - \frac{e^{i\beta_p^{(n)}h}}{2i\beta_p^{(n)}}\left(e^{i\beta_p^{(n)}h} + e^{-i\beta_p^{(n)}h}\right)\left[-2ih^{-1}\sin\left(\kappa_p h\right)\right]g^{(n)} \\
={}& \frac{\alpha_n^2 e^{i\beta_p^{(n)}h}}{i\beta_p^{(n)}\left(\alpha_n^2 + \beta_p^{(n)}\beta_s^{(n)}\right)}\left[-ih^{-1}\left(1 + \alpha_n^{-2}\beta_p^{(n)}\beta_s^{(n)}\right)\sin\left(\kappa_p h\right)\left(e^{i\beta_p^{(n)}h} + e^{-i\beta_p^{(n)}h}\right) \right. \\
&\quad \left. - 2i\alpha_n^{-2}\kappa_p\beta_p^{(n)}\beta_s^{(n)}\right]g^{(n)} - \frac{e^{i\beta_p^{(n)}h}}{2i\beta_p^{(n)}}\left(e^{i\beta_p^{(n)}h} + e^{-i\beta_p^{(n)}h}\right)\left[-2ih^{-1}\sin\left(\kappa_p h\right)\right]g^{(n)} \\
={}& \frac{e^{i\beta_p^{(n)}h}}{i\beta_p^{(n)}}\left[-ih^{-1}\sin\left(\kappa_p h\right)\left(e^{i\beta_p^{(n)}h} + e^{-i\beta_p^{(n)}h}\right) - \frac{2i\kappa_p\beta_p^{(n)}\beta_s^{(n)}}{\alpha_n^2 + \beta_p^{(n)}\beta_s^{(n)}} \right. \\
&\quad \left. + ih^{-1}\sin\left(\kappa_p h\right)\left(e^{i\beta_p^{(n)}h} + e^{-i\beta_p^{(n)}h}\right)\right]g^{(n)} \\
={}& \left(\frac{-2\kappa_p\beta_s^{(n)}}{\alpha_n^2 + \beta_p^{(n)}\beta_s^{(n)}}\right)e^{i\beta_p^{(n)}h}g^{(n)}
\end{aligned}
\tag{3.18}
$$

and

$$
\begin{aligned}
\psi_1^{(n)}(h) ={}& \frac{i\alpha_n e^{i\beta_s^{(n)}h}}{\alpha_n^2 + \beta_p^{(n)}\beta_s^{(n)}}\left\{ -e^{i\beta_p^{(n)}h}\left[-2ih^{-1}\sin\left(\kappa_p h\right)\right] \right. \\
&\quad \left. - 2i\kappa_p - 2ih^{-1}e^{i\beta_p^{(n)}h}\sin\left(\kappa_p h\right)\right\} g^{(n)} \\
={}& \left(\frac{2\kappa_p\alpha_n}{\alpha_n^2 + \beta_p^{(n)}\beta_s^{(n)}}\right)e^{i\beta_s^{(n)}h}g^{(n)}.
\end{aligned}
\tag{3.19}
$$

It is clear to note from (3.18) and (3.19) that the linear terms in the power series completely carry the profile information, i.e., the Fourier coefficient $g^{(n)}$, of the scattering surface function f.

4. Inverse scattering

Based on the transformed field expansion and analytic solutions of the leading and linear terms, we present explicit inversion formulas to reconstruct the scattering surface. The formulas differ according to different types of the input data: the decomposed data or the combined data.

4.1. Decomposed data

Let $\boldsymbol{u}_\mathrm{p}$ and $\boldsymbol{u}_\mathrm{s}$ be the compressional part and the shear part of the total field $\boldsymbol{u}$. It follows from the Helmholtz decomposition that

$$\boldsymbol{u}_\mathrm{p} = \nabla\phi, \qquad \boldsymbol{u}_\mathrm{s} = \mathbf{curl}\,\psi.$$

Assuming that the compressional and shear parts of the wavefield can be measured, we have the decomposed data

$$\begin{cases} \boldsymbol{u}_\mathrm{p}(x, h) = \left[\partial_x\phi(x, h), \ \partial_y\phi(x, h) \right], \\ \boldsymbol{u}_\mathrm{s}(x, h) = \left[\partial_y\psi(x, h), \ -\partial_x\psi(x, h) \right]. \end{cases} \tag{4.1}$$

Plugging the transparent boundary condition (2.19) into (4.1) yields

$$\begin{cases} \boldsymbol{u}_\mathrm{p}(x, h) = \left[\partial_x\phi(x, h), \ \mathscr{B}_\mathrm{p}\phi(x, h) + \rho \right], \\ \boldsymbol{u}_\mathrm{s}(x, h) = \left[\mathscr{B}_\mathrm{s}\psi(x, h), \ -\partial_x\psi(x, h) \right]. \end{cases} \tag{4.2}$$

Substituting the power series expansions for $\boldsymbol{u}_\mathrm{p}$, $\boldsymbol{u}_\mathrm{s}$, ϕ, ψ, we obtain

$$\begin{cases} \boldsymbol{u}_{\mathrm{p},k}(x, h) = \left[\partial_x\phi_k(x, h), \ \mathscr{B}_\mathrm{p}\phi_k(x, h) + \rho_k \right], \\ \boldsymbol{u}_{\mathrm{s},k}(x, h) = \left[\mathscr{B}_\mathrm{s}\psi_k(x, h), \ -\partial_x\psi_k(x, h) \right], \end{cases} \tag{4.3}$$

which gives in the frequency domain that

$$\begin{cases} \boldsymbol{u}_{\mathrm{p},k}^{(n)}(h) = \left[\mathrm{i}\alpha_n\phi_k^{(n)}(h), \ \mathrm{i}\beta_\mathrm{p}^{(n)}\phi_k^{(n)}(h) + \rho_k^{(n)} \right], \\ \boldsymbol{u}_{\mathrm{s},k}^{(n)}(h) = \left[\mathrm{i}\beta_\mathrm{s}^{(n)}\psi_k^{(n)}(h), \ -\mathrm{i}\alpha_n\psi_k^{(n)}(h) \right]. \end{cases} \tag{4.4}$$

Substituting (3.17) into (4.4) yields for $k = 0$ that

$$\boldsymbol{u}_{\mathrm{p},0}^{(n)}(h) = 2\left[\alpha_n\kappa_\mathrm{p}^{-1}\cos\left(\kappa_\mathrm{p}h\right), \ \beta_\mathrm{p}^{(n)}\kappa_\mathrm{p}^{-1}\cos\left(\kappa_\mathrm{p}h\right) - \mathrm{e}^{-\mathrm{i}\kappa_\mathrm{p}h} \right]\delta_{0n},$$
$$\boldsymbol{u}_{\mathrm{s},0}^{(n)}(h) = [0, \ 0],$$

which implies that

$$\boldsymbol{u}_{\mathrm{p},0}(x, h) = \left[0, \ 2\mathrm{i}\sin\left(\kappa_\mathrm{p}h\right) \right], \qquad \boldsymbol{u}_{\mathrm{s},0}(x, h) = [0, \ 0].$$

Substituting (3.18) and (3.19) into (4.4) gives for $k = 1$ that

$$\boldsymbol{u}_{\mathrm{p},1}^{(n)}(h) = -2\mathrm{i}\kappa_\mathrm{p}\beta_\mathrm{s}^{(n)}\left(\alpha_n^2 + \beta_\mathrm{p}^{(n)}\beta_\mathrm{s}^{(n)} \right)^{-1}\left[\alpha_n, \ \beta_\mathrm{p}^{(n)} \right]\mathrm{e}^{\mathrm{i}\beta_\mathrm{p}^{(n)}h}g^{(n)},$$
$$\boldsymbol{u}_{\mathrm{s},1}^{(n)}(h) = 2\mathrm{i}\kappa_\mathrm{p}\alpha_n\left(\alpha_n^2 + \beta_\mathrm{p}^{(n)}\beta_\mathrm{s}^{(n)} \right)^{-1}\left[\beta_\mathrm{s}^{(n)}, \ -\alpha_n \right]\mathrm{e}^{\mathrm{i}\beta_\mathrm{s}^{(n)}h}g^{(n)}.$$

Although either $\boldsymbol{u}_{\mathrm{p},1}^{(n)}(h)$ or $\boldsymbol{u}_{\mathrm{s},1}^{(n)}(h)$ gives an explicit relation to the Fourier coefficient of the surface profile function $g^{(n)}$ and is readily to derive the reconstruction formula, it is not convenient to use in practice. In fact, a simple calculation yields

$$\mathrm{e}^{-\mathrm{i}\beta_\mathrm{p}^{(n)}h}\boldsymbol{u}_{\mathrm{p},1}^{(n)}(h) + \mathrm{e}^{-\mathrm{i}\beta_\mathrm{s}^{(n)}h}\boldsymbol{u}_{\mathrm{s},1}^{(n)}(h) = \left[0, \ -2\mathrm{i}\kappa_\mathrm{p} \right]g^{(n)}, \tag{4.5}$$

which is simple and may lead to an elegant reconstruction formula.

4.2. Combined data

Alternatively, we consider the combined data $\boldsymbol{u}(x, h) = [u_1(x, h), \ u_2(x, h)]$ itself in case that its compressional and shear parts may not be available.

It follows from the Helmholtz decomposition (2.7) that we have

$$
\begin{cases}
u_1(x, h) = \partial_x \phi(x, h) + \partial_y \psi(x, h), \\
u_2(x, h) = \partial_y \phi(x, h) - \partial_x \psi(x, h).
\end{cases}
\tag{4.6}
$$

Substituting the transparent boundary conditions (2.19) into (4.6) yields

$$
\begin{cases}
u_1(x, h) = \partial_x \phi(x, h) + \mathscr{B}_s \psi(x, h), \\
u_2(x, h) = \mathscr{B}_p \phi(x, h) - \partial_x \psi(x, h) + \rho.
\end{cases}
\tag{4.7}
$$

Consider the power series expansion for u_j:

$$
u_j(x, y; \varepsilon) = \sum_{k=0}^{\infty} u_{j,k}(x, y) \varepsilon^k.
\tag{4.8}
$$

Using the power series expansions of u_j, ϕ, ψ, we obtain from (4.7) that

$$
\begin{cases}
u_{1,k}(x, h) = \partial_x \phi_k(x, h) + \mathscr{B}_s \psi_k(x, h), \\
u_{2,k}(x, h) = \mathscr{B}_p \phi_k(x, h) - \partial_x \psi_k(x, h) + \rho_k,
\end{cases}
\tag{4.9}
$$

where $\rho_0 = \rho$, $\rho_k = 0$ for $k > 0$. Comparing the Fourier coefficients in the frequency domain of (4.9) gives

$$
\begin{cases}
u_{1,k}^{(n)}(h) = \mathrm{i}\alpha_n \phi_k^{(n)}(h) + \mathrm{i}\beta_s^{(n)} \psi_k^{(n)}(h), \\
u_{2,k}^{(n)}(h) = \mathrm{i}\beta_p^{(n)} \phi_k^{(n)}(h) - \mathrm{i}\alpha_n \psi_k^{(n)}(h) + \rho_k^{(n)}.
\end{cases}
\tag{4.10}
$$

Substituting (3.17) into (4.10) yields for $k = 0$ that

$$
u_{1,0}^{(n)}(h) = 2\kappa_p^{-1} \alpha_n \cos\left(\kappa_p h\right) \delta_{0n},
$$

$$
u_{2,0}^{(n)}(h) = 2\left[\kappa_p^{-1} \beta_p^{(n)} \cos\left(\kappa_p h\right) - \mathrm{e}^{-\mathrm{i}\kappa_p h}\right] \delta_{0n},
$$

which implies that

$$
u_{1,0}(x, h) = 0, \quad u_{2,0}(x, h) = 2\mathrm{i} \sin\left(\kappa_p h\right).
\tag{4.11}
$$

Substituting (3.18) and (3.19) into (4.10) gives for $k = 1$ that

$$
u_{j,1}^{(n)}(h) = M_j^{(n)} g^{(n)},
\tag{4.12}
$$

where

$$
M_1^{(n)} = \frac{2\mathrm{i}\kappa_p \alpha_n \beta_s^{(n)}}{\alpha_n^2 + \beta_p^{(n)} \beta_s^{(n)}} \left(\mathrm{e}^{\mathrm{i}\beta_s^{(n)} h} - \mathrm{e}^{\mathrm{i}\beta_p^{(n)} h}\right),
$$

$$
M_2^{(n)} = \frac{-2\mathrm{i}\kappa_p}{\alpha_n^2 + \beta_p^{(n)} \beta_s^{(n)}} \left(\beta_p^{(n)} \beta_s^{(n)} \mathrm{e}^{\mathrm{i}\beta_p^{(n)} h} + \alpha_n^2 \mathrm{e}^{\mathrm{i}\beta_s^{(n)} h}\right).
$$

Again, it is not convenient to use (4.12) in the reconstruction formula. It is easy to note that

$$\alpha_n \left(\beta_s^{(n)} \right)^{-1} M_1^{(n)} + M_2^{(n)} = -2i\kappa_p e^{i\beta_p^{(n)}h}.$$

Combining (4.12) and the above identity, we deduce

$$\alpha_n \left(\beta_s^{(n)} \right)^{-1} u_{1,1}^{(n)}(h) + u_{2,1}^{(n)}(h) = -2i\kappa_p e^{i\beta_p^{(n)}h} g^{(n)}, \tag{4.13}$$

which is simple and may also lead to an elegant reconstruction formula.

4.3. Reconstruction formula

In practice, the combined data may be easier to get than the decomposed data. We shall derive an explicit reconstruction formula based on the combined data. An alternative reconstruction formula can be deduced similarly for the decomposed data.

Due to the presence of noise, the scattering data is assumed to have the form:

$$u_j^\delta(x, h) = u_j(x, h) + \mathcal{O}(\delta), \tag{4.14}$$

where $u_j(x, h)$ is the noise-free data and δ is the noise level.

It follows from the power series expansion (4.8) that

$$u_j^\delta(x, h) = u_{j,0}(x, h) + \varepsilon u_{j,1}(x, h) + e_j, \tag{4.15}$$

where $e_j = \mathcal{O}(\varepsilon^2)$ stands for the remaining higher order terms substituting the noise data (4.14) into (4.15) yields

$$u_j(x, h) = u_{j,0}(x, y) + \varepsilon u_{j,1}(x, h) + \mathcal{O}\left(\varepsilon^2\right) + \mathcal{O}(\delta).$$

Dropping the higher order and noise terms, we linearize the nonlinear inverse problem and obtain

$$\varepsilon u_{j,1}(x, h) = u_j^\delta(x, h) - u_{j,0}(x, h). \tag{4.16}$$

Combining (4.13) and (4.16) yields

$$\alpha_n \left(\beta_s^{(n)} \right)^{-1} \left(u_1^{\delta(n)}(h) - u_{1,0}^{(n)}(h) \right) + \left(u_2^{\delta(n)}(h) - u_{2,0}^{(n)}(h) \right) = -2i\kappa_p e^{i\beta_p^{(n)}h} f^{(n)},$$

where $u_1^{\delta(n)}(h)$ and $u_2^{\delta(n)}(h)$ are the Fourier coefficients of the scattering data, and $f^{(n)}$ is the Fourier coefficient of the scattering surface function f. Hence we have an explicit representation for the Fourier coefficient of the scattering surface function:

$$
\begin{aligned}
f^{(n)} &= -\left(2i\kappa_p\right)^{-1} \left[\alpha_n \left(\beta_s^{(n)} \right)^{-1} \left(u_1^{\delta(n)}(h) - u_{1,0}^{(n)}(h) \right) + \left(u_2^{\delta(n)}(h) - u_{2,0}^{(n)}(h) \right) \right] e^{-i\beta_p^{(n)}h} \\
&= -\left(2i\kappa_p\right)^{-1} \left[\left(\alpha_n \left(\beta_s^{(n)} \right)^{-1} u_1^{\delta(n)}(h) + u_2^{\delta(n)}(h) \right) - u_{2,0}^{(n)}(h) \right] e^{-i\beta_p^{(n)}h}.
\end{aligned}
\tag{4.17}
$$

It is easy to observe from $\beta_p^{(n)}$ that it is well-posed to reconstruct those Fourier coefficients $f^{(n)}$ for $|\alpha_n| < \kappa_p$. The reason is that the noise is controllable and will not contaminate the reconstruction largely. However, the resolution of the reconstructed function f is limited by the given compressional wavenumber κ_p. Contrastly, it is severely ill-posed to reconstruct those Fourier coefficients $f^{(n)}$ with $|\alpha_n| > \kappa_p$ since a small amount of noise will be exponentially enlarged and lead to huge errors in the reconstruction. Nonetheless, these evanescent wave components contribute to the super resolution of the reconstructed function f. It is

crucial to suppress the exponetial growth of the error while still maintain the super-resolved resolution.

Following [11], we consider a spectral cut-off regularization

$$f^{(n)} = -\left(2i\kappa_{\mathrm{p}}\right)^{-1}\left[\left(\alpha_n\left(\beta_{\mathrm{s}}^{(n)}\right)^{-1}u_1^{\delta(n)}(h) + u_2^{\delta(n)}(h)\right) - u_{2,0}^{(n)}(h)\right]e^{-i\beta_{\mathrm{p}}^{(n)}h}\chi_{[-\kappa_{\mathrm{c}},\,\kappa_{\mathrm{c}}]}(\alpha_n), \quad (4.18)$$

where the characteristic function

$$\chi_{[-\kappa_{\mathrm{c}},\,\kappa_{\mathrm{c}}]}(\alpha_n) = \begin{cases} 1, & \text{for } |\alpha_n| < \kappa_{\mathrm{c}}, \\ 0, & \text{for } |\alpha_n| > \kappa_{\mathrm{c}}. \end{cases}$$

Here $\kappa_{\mathrm{c}} > \kappa_{\mathrm{p}}$ is the cut-off wavenumber and may be determined from the signal-to-noise ratio. Once the Fourier coefficient $f^{(n)}$ is computed, the scattering surface function can be approximated by

$$\begin{aligned} f(x) &\approx \sum_{n\in\mathbb{Z}} f^{(n)}\,e^{i\alpha_n x} = -\left(2i\kappa_{\mathrm{p}}\right)^{-1}\sum_{|\alpha_n|<\kappa_{\mathrm{c}}}\left[\left(\alpha_n\left(\beta_{\mathrm{s}}^{(n)}\right)^{-1}u_1^{\delta(n)}(h) + u_2^{\delta(n)}(h)\right)\right.\\ &\quad \left. - u_{2,0}^{(n)}(h)\right]e^{i\left(\alpha_n x - \beta_{\mathrm{p}}^{(n)}h\right)} \\ &= -\left(2i\kappa_{\mathrm{p}}\right)^{-1}\sum_{|\alpha_n|<\kappa_{\mathrm{c}}}\left[\left(\alpha_n\left(\beta_{\mathrm{s}}^{(n)}\right)^{-1}u_1^{\delta(n)}(h) + u_2^{\delta(n)}(h)\right)e^{i\left(\alpha_n x - \beta_{\mathrm{p}}^{(n)}h\right)}\right.\\ &\quad + \kappa_{\mathrm{p}}^{-1}\sin\left(\kappa_{\mathrm{p}}h\right)e^{-i\kappa_{\mathrm{p}}h}. \end{aligned} \quad (4.19)$$

Hence, the method requires only two FFT: one is done for the data to obtain the Fourier coefficients of the scattering data $u_1^{\delta(n)}(h)$ and $u_2^{\delta(n)}(h)$ and another is taken to obtain the reconstructed scattering function f.

5. Numerical experiments

In this section we discuss the implementation of the direct and inverse problems. We report the numerical results for three types of surfaces: a periodic smooth surface, a locally perturbed smooth surface, and two non-smooth surfaces. We shall investigate the dependence of the results on the following parameters: the measurement distance h, the noise level δ, and the surface deformation parameter ε.

5.1. Direct solver

We use the finite element method and directly solve the boundary value problem (2.28) to obtain the synthetic data for the inverse problem. Although the transparent boundary condition (2.27) is exact, it is nonlocal and inconvenient to implement in practice. Computationally, we adopt the local PML technique to truncate the domain in the *y*-direction [16].

Consider the Navier equation for the scattered field in Ω:

$$\mu\Delta v + (\lambda + \mu)\nabla\nabla \cdot v + \omega^2 v = 0,$$

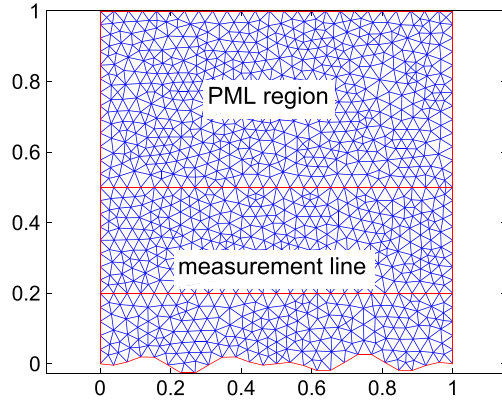**Figure 2.** A typical diagram of the computational domain for the PML problem.

whose component-wise version is

$$(\lambda + 2\mu)\partial_{xx}v_1 + \mu\partial_{yy}v_1 + (\lambda + \mu)\partial_{xy}v_2 + \omega^2 v_1 = 0,$$

$$\mu\partial_{xx}v_2 + (\lambda + 2\mu)\partial_{yy}v_2 + (\lambda + \mu)\partial_{xy}v_1 + \omega^2 v_2 = 0.$$

Denote the computational domain $\Omega^{\text{PML}} = \{(x, y) \in \mathbb{R}^2 : f(x) < y < h + d, \ 0 < x < \Lambda\}$, where $d > 0$ is the PML thickness. Define $\Gamma^{\text{PML}} = \{(x, y) \in \mathbb{R}^2 : y = h + d, \ 0 < x < \Lambda\}$. Let $s(y) = 1 + i\sigma(y)$ be the model medium property, where σ is a positive continuous function satisfying $\sigma(y) = 0$ in Ω. Following the general idea in designing the PML absorbing layer, we may deduce the truncated PML equations:

$$(\lambda + 2\mu)\partial_x\big(s\partial_x v_1\big) + \mu\partial_y\big(s^{-1}\partial_y v_1\big) + (\lambda + \mu)\partial_{xy}v_2 + s\omega^2 v_1 = 0,$$

$$\mu\partial_x\big(s\partial_x v_2\big) + (\lambda + 2\mu)\partial_y\big(s^{-1}\partial_y v_2\big) + (\lambda + \mu)\partial_{xy}v_1 + s\omega^2 v_2 = 0,$$

along with the Dirichlet boundary conditions

$$\boldsymbol{v} = -\boldsymbol{u}^{\text{inc}} \quad \text{on } \Gamma_f \quad \text{and} \quad \boldsymbol{v} = 0 \quad \text{on } \Gamma^{\text{PML}}.$$

Clearly, the PML equations are coupled due to the terms $\partial_{xy}v_1$ and $\partial_{xy}v_2$. We consider the following Gauss–Seidel iterative scheme to decouple the PML equations:

$$(\lambda + 2\mu)\partial_x\big(s\partial_x v_1^{(m)}\big) + \mu\partial_y\big(s^{-1}\partial_y v_1^{(m)}\big) + s\omega^2 v_1^{(m)} = -(\lambda + \mu)\partial_{xy}v_2^{(m-1)},$$

$$\mu\partial_x\big(s\partial_x v_2^{(m)}\big) + (\lambda + 2\mu)\partial_y\big(s^{-1}\partial_y v_2^{(m)}\big) + s\omega^2 v_2^{(m)} = -(\lambda + \mu)\partial_{xy}v_1^{(m)}.$$

Hence two PML equations for the Helmholtz problem need to be solved at each iteration.

For periodic scattering surface and normal incident wave, the solution of the direct problem is also periodic so that we truncate the domain in the *x*-direction by imposing the periodic boundary condition on the left and right boundaries. For locally perturbed scattering surface, we focus on the cases when the surface is symmetric about the centerline of the domain. Due to the symmetry of the domain and the incident field, the solution of the direct problem is also symmetric so that the periodic boundary condition can still be used in the *x*-direction.

As mentioned in section 4, we may present two reconstruction formulas based on either the decomposed or the combined data. Since the two formulas are mathematically equivalent
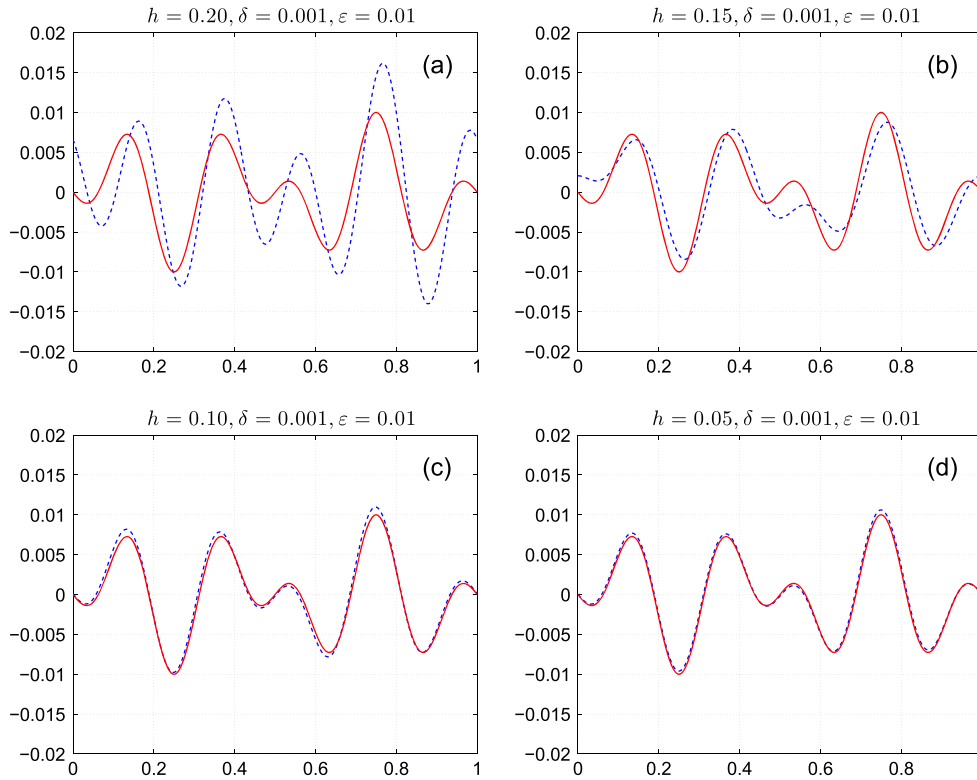
Figure 3. Example 1: computed (dashed line) against exact (solid line) solution for a periodic surface. Parameters are $\varepsilon = 0.01$, $\delta = 0.1\%$ and (a) $h = 0.2$; (b) $h = 0.15$; (c) $h = 0.1$; (d) $h = 0.05$.

and the combined data is easier to obtain in practice, we focus on this case and use only the reconstruction formula (4.19). In the following experiments, we fix the angular frequency $\omega = \pi$, the Lamé constants $\lambda = 2$ and $\mu = 1$. So the wavenumber $\kappa_p = \pi/2$ and $\kappa_s = \pi$, which correspond to the compressional wavelength 4 and the shear wavelength 2. The incident wave is taken as a single compressional plane wave at normal incidence, i.e. $u^{in} = [0, \ -1] e^{-i\kappa_p y}$. The computational domain for the direct problem is chosen to be $[0, \ 1] \times [f, \ 1]$ with the PML region $[0, \ 1] \times [0.5, \ 1]$, as shown in figure 2. After the direct problem is solved and the value of $u(x, h)$ is obtained at the grid points, a natural cubic spline interpolation is used to generate the synthetic data $u(x_i, h)$ at 513 uniformly distributed points on the line $[0, 1] \times h$. To test the stability of our method, an amount of noise is added to the data

$$u^\delta(x_i, \ h) = u(x_i, \ h)(1 + \delta \ \text{rand}),$$

where rand is independently and uniformly distributed random numbers in $[-1, 1]$.

5.2. Numerical examples

We consider three numerical experiments which include both smooth and non-smooth surfaces to illustrate the performance of the proposed method.
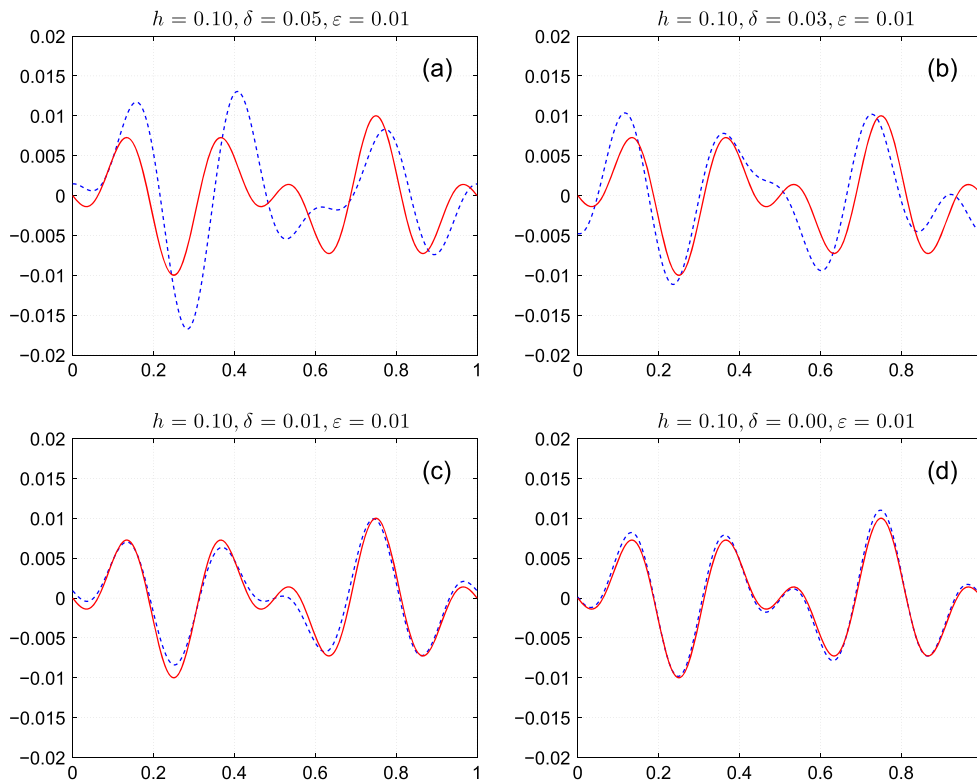
Figure 4. Example 1: computed (dashed line) against exact (solid line) solution for a periodic surface. Parameters are $\varepsilon = 0.01$, $h = 0.1$ and (a) $\delta = 5\%$; (b) $\delta = 3\%$; (c) $\delta = 1\%$; (d) $\delta = 0\%$.

Example 1. Consider a smooth surface with only two Fourier modes. The exact surface function is given by $f(x) = \varepsilon g(x)$, where

$$g(x) = 0.5 \sin(6\pi x) - 0.5 \sin(10\pi x).$$

We first consider the dependence of the resolution on the measurement height h. The deformation parameter is fixed at $\varepsilon = 0.01$ and the noise level is fixed at $\delta = 0.1\%$. We solve the inverse scattering problem by using the scattering data measured at four different height $h = 0.2, 0.15, 0.1, 0.05$. Figure 3 shows the numerical results, where the computed scattering surface (dashed line) is plotted against the exact surface (solid line) for each measurement height. Clearly better reconstruction is obtained by using smaller measurement height h. All the fine features of the scattering surface is completely recovered and subwavelength resolution is achieved, especially when using $h < 0.15$. As can be seen in the reconstruction formula (4.19), smaller h results in smaller amplification of the data noise and linearization error, as well as larger cut-off frequency. Physically speaking, by measuring closer to the surface we obtain more accurate data of the evanescent wave, which decays exponentially in the y-direction.

Next we consider the effect of the noise level δ on the reconstruction. The deformation parameter is fixed at $\varepsilon = 0.01$ and the measurement height is fixed at $h = 0.1$. Four different noise level $\delta = 5, 3, 1, 0\%$ are added to the scattering data and the results are shown in figure 4. As expected smaller noise level results in better computed solution. It is worth
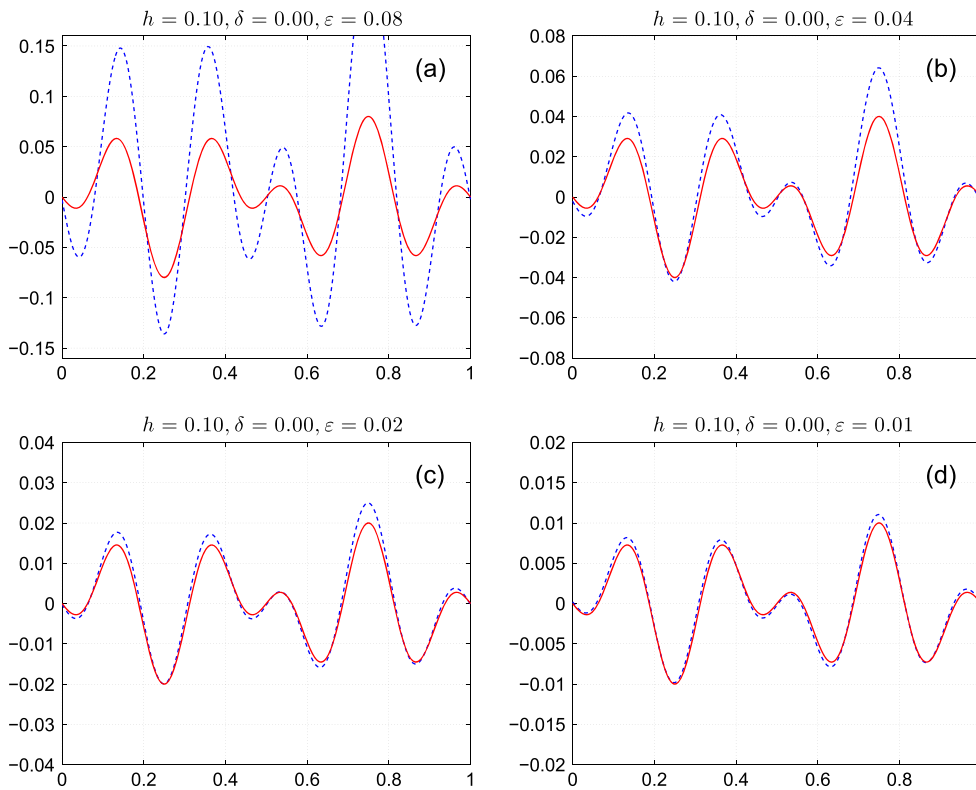
Figure 5. Example 1: computed (dashed line) against exact (solid line) solution for a periodic surface. Parameters are $h = 0.1$, $\delta = 0\%$ and (a) $\varepsilon = 0.08$; (b) $\varepsilon = 0.04$; (c) $\varepsilon = 0.02$; (d) $\varepsilon = 0.01$.

pointing out that the sensitivity of the reconstruction on the measurement noise depends on the sampling rate (the number of measurement points). Higher sampling rate results in lower sensitivity, i.e. higher tolerance of the reconstruction on the measurement noise. In our opinion this is a great advantage of the method thanks to the explicit relation between the Fourier coefficients of the data and the solution.

Finally we consider the surface deformation parameter ε. The measurement height is fixed at $h = 0.1$ and the noise level is fixed at $\delta = 0\%$, i.e. no noise is added to the data. Figure 5 shows the results with four different deformation parameter $\varepsilon = 0.08, 0.04, 0.02, 0.01$. It is clear that better reconstruction is obtained with smaller deformation parameter. This is reasonable since ε implies smaller linearization error $\mathcal{O}(\varepsilon^2)$ when we drop the higher order terms in the power series expansion.

Example 2. Consider a smooth surface with infinitely many Fourier modes. The exact surface deformation function is given by $f(x) = \varepsilon g(x)$, where

$$g(x) = \{\cos[6\pi(x - 0.5)] - \cos[10\pi(x - 0.5)]\}e^{-25(x-0.5)^2}.$$

Since the observations on the effect of the parameters h, ε, and δ are similar as those in example 1, we shall not repeat all experiments but only present some representative results. Figure 6 shows the results for four different set of parameters. Again we are able to achieve subwavelength resolution as long as the parameters are sufficiently small.
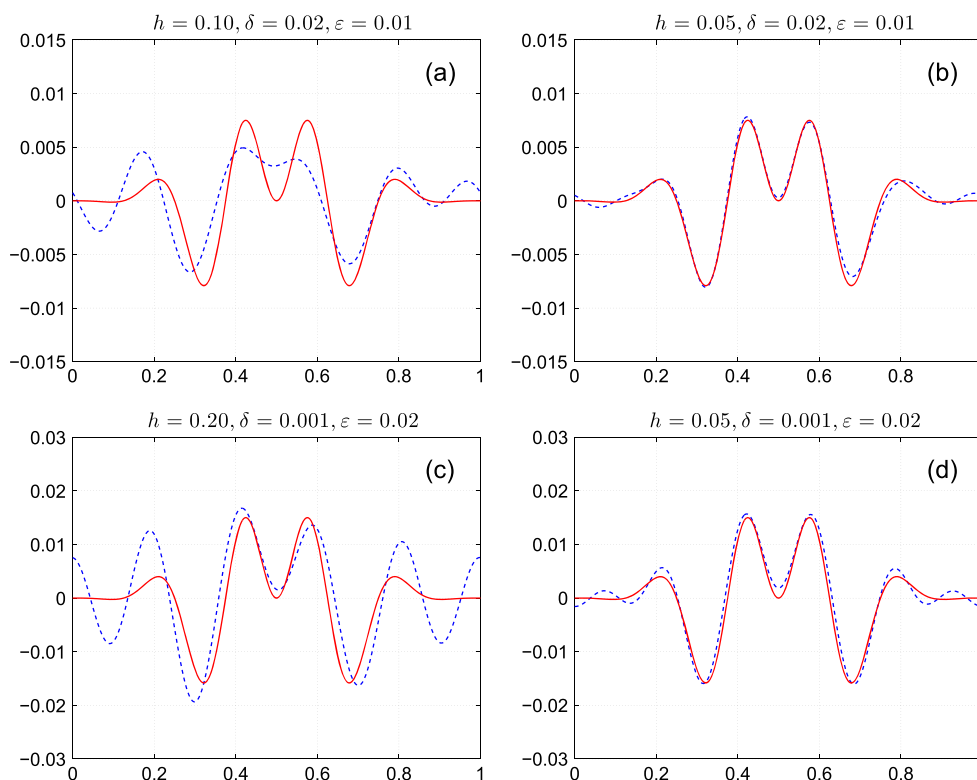
Figure 6. Example 2: computed (dashed line) against exact (solid line) solution for a locally perturbed surface. Parameters are (a) $h = 0.1$, $\delta = 2\%$, $\varepsilon = 0.01$; (b) $h = 0.05$, $\delta = 2\%$, $\varepsilon = 0.01$; (c) $h = 0.2$, $\delta = 0.1\%$, $\varepsilon = 0.02$; (d) $h = 0.05$, $\delta = 0.1\%$, $\varepsilon = 0.02$.

Example 3. We demonstrate that our method can also be applied to non-smooth surfaces, although the mathematical justification requires that the surface belongs to C^2. We consider two examples. The first exact surface deformation function is given by $f(x) = \varepsilon g(x)$, where

$$g(x) = (1 - 10\,|x - 0.3|)\chi_{[0.2, 0.4]} + (1 - 10\,|x - 0.7|)\chi_{[0.6, 0.8]},$$

where χ denotes the characteristic function. The second exact surface deformation function is given by $f(x) = \varepsilon g(x)$, where

$$g(x) = \chi_{[0.2, 0.4]} + \chi_{[0.6, 0.8]}.$$

Again we shall not present all investigations on the parameters but just report a few representative results to show the effectiveness of the method. Figure 7 shows the results for the two scattering surfaces, each with two sets of parameters. The quality of the reconstruction for the non-smooth but continuous surface is as good as those for the smooth surfaces. The reconstruction of the discontinuous surface displays the well known Gibbs phenomenon around the points of discontinuities.
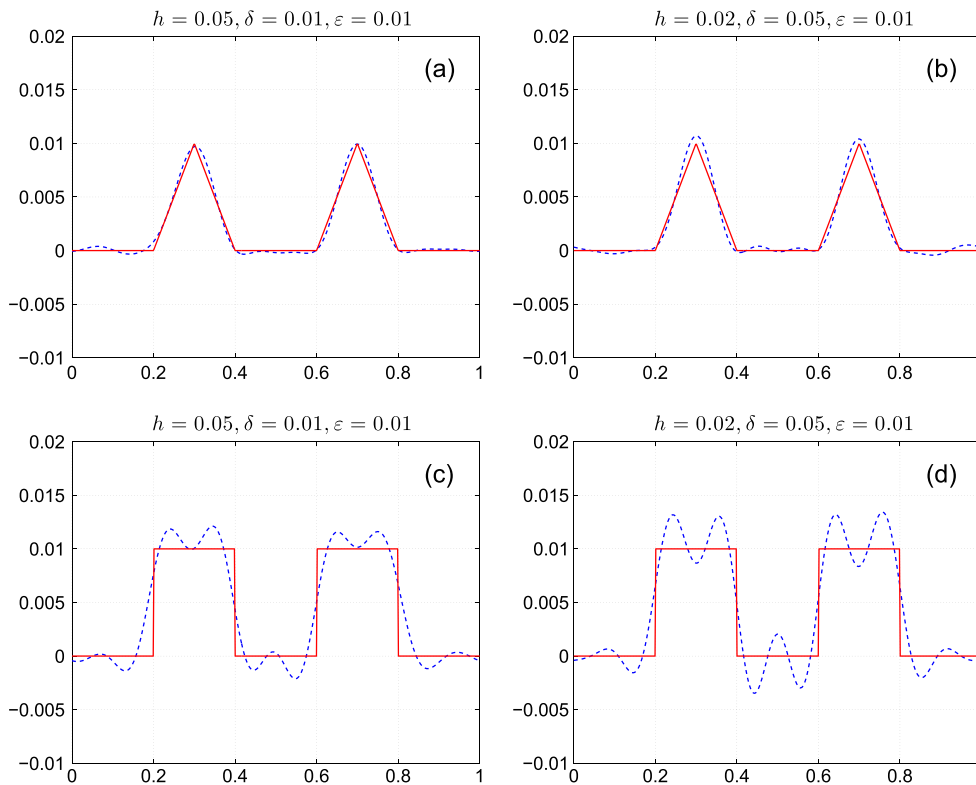
Figure 7. Example 3: computed (dashed line) against exact (solid line) solution for non-smooth surfaces. Parameters are (a) $h = 0.05$, $\delta = 1\%$, $\varepsilon = 0.01$; (b) $h = 0.02$, $\delta = 5\%$, $\varepsilon = 0.01$; (c) $h = 0.05$, $\delta = 1\%$, $\varepsilon = 0.01$; (d) $h = 0.02$, $\delta = 5\%$, $\varepsilon = 0.01$.

6. Concluding remarks

We presented a simple, effective, and efficient method for solving an inverse problem of surface scattering by elastic wave with near-field data. The surface was assumed to be a small and smooth deformation of the ground plane. A crucial step was to decompose the total field into its compressional and shear parts via the Helmholtz decomposition. The transformed field expansion was applied to each part and a recursive boundary value problem for the power series expansions is derived. These boundary value problems were coupled at the lower boundary line of the transformed domain. After solving analytically the coupled system and dropping high order terms in the power series expansion, the inverse problem was linearized and explicit reconstruction formulas were deduced for both the decomposed data and the combined data. The method requires only a single illumination at a fixed frequency and incident angle and is realized efficiently by the FFT. Although the presentation was for periodic surfaces, it could be translated directly to more general rough surfaces. In numerical experiments, we investigated three types of surfaces: periodic, locally perturbed, and non-smooth. The results show that our method is effective in reconstructing those surfaces with subwavelength. We also examined the effects of various parameters and found that smaller

measurement distance, lower noise level, and smaller deformation parameter would yield more accurate results.

As for future work, we plan to extend the method to solve the inverse surface scattering problem with other boundary conditions, transmission problems where the surface is penetrable, and inverse obstacle or cavity scattering problems. Other interesting and challenging problems include the three-dimensional problem, random surfaces, phaseless or limited aperture data, as well convergence analysis of the method.

Appendix. A two-point boundary value problem

Consider the two-point boundary value problem

$$
\begin{cases}
w'' + \beta^2 w = v, & 0 < y < h, \\
w' = r, & y = 0, \\
w' - i\beta w = s, & y = h,
\end{cases}
\tag{A.1}
$$

where $\beta \neq 0$ is a constant.

Using the integrated solution method (see, [11, lemma B.1]), we may obtain the analytic solution for the two-point boundary value problem (A.1).

Lemma Appendix A.1. *The two-point boundary value problem (A.1) has a unique solution, given by*

$$
w(y) = K_1(y; \beta) r - K_2(y; \beta) s + \int_0^h K_3(y, z; \beta) v(z) \mathrm{d}z,
$$

where

$$
K_1(y; \beta) = \frac{\mathrm{e}^{i\beta y}}{i\beta}, \quad K_2(y; \beta) = \frac{\mathrm{e}^{i\beta h}}{2i\beta}\left(\mathrm{e}^{i\beta y} + \mathrm{e}^{-i\beta y}\right),
$$

and

$$
K_3(y, z; \beta) =
\begin{cases}
\dfrac{\mathrm{e}^{i\beta y}}{2i\beta}\left(\mathrm{e}^{i\beta z} + \mathrm{e}^{-i\beta z}\right), & z < y, \\[2ex]
\dfrac{\mathrm{e}^{i\beta z}}{2i\beta}\left(\mathrm{e}^{i\beta y} + \mathrm{e}^{-i\beta y}\right), & z > y.
\end{cases}
$$

References

[1] Abubakar I 1962 Scattering of plane elastic waves at rough surfaces *Proc. Camb. Phil. Soc.* **58** 136–57
[2] Alves C and Ammari H 2001 Boundary integral formula for the reconstruction of imperfections of small diameter in an elastic medium *SIAM J. Appl. Math.* **62** 94–106
[3] Ammari H and Kang H 2004 Reconstruction of small inhomogeneities from boundary measurements *Lecture Notes in Mathematics* vol 1846 (Berlin: Springer)
[4] Ammari H, Kang H, Nakamura G and Tanuma K 2002 Complete asymptotic expansions of solutions of the system of elastostatics in the presence of inhomogeneities of small diameter *J. Elast.* **67** 97–129
[5] Charalambopoulos A, Gintides D and Kiriaki K 2001 On the uniqueness of the inverse elastic scattering problem for periodic structures *Inverse Problems* **17** 1923–35

  [6] Arens T 1999 The scattering of plane elastic waves by a one-dimensional periodic surface *Math. Methods Appl. Sci.* **22** 55–72

  [7] Arens T 1999 A new integral equation formulation for the scattering of plane elastic waves by diffraction gratings *J. Integral Equ. Appl.* **11** 275–97

  [8] Arens T 2001 Uniqueness for elastic wave scattering by rough surfaces *SIAM J. Math. Anal.* **33** 461–76

  [9] Arens T 2002 Existence of solution in elastic wave scattering by unbounded rough surfaces *Math. Methods Appl. Sci.* **25** 507–28

  [10] Bao G, Cui T and Li P 2014 Inverse diffraction grating of Maxwell's equations in biperiodic structures *Opt. Express* **22** 4799–816

  [11] Bao G and Li P 2013 Near-field imaging of infinite rough surfaces *SIAM J. Appl. Math.* **73** 2162–87

  [12] Bao G and Li P 2014 Near-field imaging of infinite rough surfaces in dielectric media *SIAM J. Imaging Sci.* **7** 867–89

  [13] Bao G and Li P 2014 convergence analysis in near-field imaging *Inverse Problems* **30** 085008

  [14] Bonnet M and Constantinescu A 2005 Inverse problems in elasticity *Inverse Problems* **21** 1–50

  [15] Cheng T, Li P and Wang Y 2013 Near-field imaging of perfectly conducting grating surfaces *J. Opt. Soc. Am.* A **30** 2473–81

  [16] Chen Z and Wu H 2003 An adaptive finite element method with perfectly matched absorbing layers for the wave scattering by periodic structures *SIAM J. Numer. Anal.* **41** 799–826

  [17] Elschner J and Hu G 2010 Variational approach to scattering of plane elastic waves by diffraction gratings *Math. Methods Appl. Sci.* **33** 1924–41

  [18] Elschner J and Hu G 2012 An optimization method in inverse elastic scattering for one-dimensional grating profiles *Commun. Comput. Phys.* **12** 1434–60

  [19] Elschner J and Hu G 2012 Scattering of plane elastic waves by three-dimensional diffraction gratings *Math. Models Methods Appl. Sci.* **22** 1150019

  [20] Elschner J and Hu G 2012 Elastic scattering by unbounded rough surfaces *SIAM J. Math. Anal.* **44** 4101–27

  [21] Elschner J and Hu G 2015 Elastic scattering by unbounded rough surfaces: solvability in weighted Sobolev spaces *Appl. Anal.* **94** 251–78

  [22] Fokkema J 1980 Reflection and transmission of elastic waves by the spatially periodic interface between two solids (theory of the integral-equation method) *Wave Motion* **2** 375–93

  [23] Fokkema J and Van Den Berg P M 1977 Elastodynamic diffraction by a periodic rough surface (stress-free boundary) *J. Acoust. Soc. Am.* **62** 1095–101

  [24] Hu G, Lu Y and Zhang B 2013 The factorization method for inverse elastic scattering from periodic structures *Inverse Problems* **29** 115005

  [25] Landau L D and Lifshitz E M 1986 *Theory of Elasticity* (Oxford, UK: Pergamon)

  [26] Li P and Wang Y 2015 Near-field imaging of obstacles *Inverse Problems and Imaging* **9** 189–210

  [27] Li P and Wang Y 2015 Near-field imaging of interior cavities *Commun. Comput. Phys.* **17** 542–63

  [28] Santosa F (ed) 1984 *Inverse Problems of Acoustic and Elastic Waves* (Philadelphia: SIAM)

  [29] Sherwood J W C 1958 Elastic wave propagation in a semi-infinite solid medium *Proc. Phys. Soc.* **71** 207–19